CHAPTER 6: EARTHQUAKE PROBABILITIES FOR THE SAN FRANCISCO BAY REGION 2002—2031: RESULTS AND DISCUSSION

Introduction

Here we report and discuss earthquake probabilities calculated from the methods and inputs developed in the preceding chapters. As indicated in the adjoining box, we report probabilities for several different types of sources, and for various time periods and magnitudes of interest. A full description of the earthquake probability in the SFBR earthquake model includes estimates of the mean magnitude and probability for each rupture source (including single- and multi-segment ruptures), of the probability for rupture involving a particular fault segment (which may involve earthquakes of different sizes), and of the probability of earthquakes above a specified magnitude on each *fault system*, in the *background*, and in the *region*. We focus on the probabilities of **M**≥6.7 earthquakes. We also quantify and discuss rupture probabilities for earthquakes having **M**<6.7. The regional probabilities reported here refer to earthquakes occurring within the geographic bounds of the SFBR. While some earthquakes in our model occur outside the SFBR (on the off-shore segment of the San Andreas fault), we include in the regional and fault system results only earthquakes that rupture one or more segments within the SFBR and floating earthquakes that occur within the region.

Because our calculations employ a Monte Carlo method, we report each probability as a mean value and the associated 95% confidence bound, the latter shown as a range printed within square brackets[1]. The mean values are our principal results, while the confidence bounds define the formal uncertainties in the probability calculations (as described in Chapter 5). When we refer simply to "the probability", we are referring to the mean 30-year probability. The width of the confidence bounds reflects the uncertainty in both the models and the input parameters used in the calculations.

As described in Chapter 5, we employed a suite of probability models in our calculations: Poisson, Brownian Passage Time (BPT), Time-predictable (TP) and Empirical. Our principal results reflect weighted averages of these models. To explore the implications for some of the modeling assumptions, we will from time to time refer to or compare calculations for individual probability models throughout this chapter.

We focus on the 30-year time window 2002-2031 but also report results for other intervals of interest to the community, including probabilities in 1-, 5-, 10-, and 20-year intervals calculated with our weighted (preferred) model, and in a 100-year interval (2002-2102) calculated with the time-independent, Poisson model. We also determine the probabilities for **M**≥7.0 and **M**≥7.5 earthquakes on each fault and in the region. Unlike WG88 and WG90. which stated

[1] For example, if a result is given as 0.62 [0.38 – 0.85], then 2.5% of the viable models in the calculation had probabilities less than 0.38 and 2.5% had probabilities greater than 0.85.

probabilities for earthquakes having magnitudes of about 7 or about 8, this study is precise about earthquake magnitudes for each rupture source.

In what follows, the section on **Regional Earthquake Probabilities** presents results for the region and its major sub-regions, and for various magnitude thresholds and time periods. Next, the section on **Individual Faults and the Background** examines earthquake probabilities for each of the characterized fault systems and the background, and examines each fault's setting and the key factors involved in shaping the results. The section on **Comparison to Earlier Probability Reports** examines some of the reasons for the differences between this report and earlier ones. The section on **Sensitivity of the Results** examines the dependence of the results on some of the assumptions made in the model and uncertainties encountered in the data.

Probability Of What?

Earthquake probabilities are presented in this chapter for each of the five cases defined below.

Fault segments. The 18 fault segments are the building blocks of the rupture sources. When a fault segment ruptures, the rupture may be confined to the segment, or it may involve two or more adjacent segments. Hence, ruptures of a given fault segment can involve earthquakes with a wide range of magnitudes. The probability of fault segment rupture refers to the chance the segment will rupture, regardless (unless otherwise stated) of the size of the earthquake involved. Segment rupture probabilities are shown in the left half of **Table 6.3** and the middle sections of **Tables 6.4-6.10**. The right half of **Table 6.3** shows corresponding fault segment probabilities for **M**≥6.7 earthquakes.

Rupture sources. A rupture source comprises a specified set of (one or more) fault segments. For some faults the term also includes 'floating earthquakes'. Each rupture source generates earthquakes having a distinct mean magnitude governed by its geometry. In the SFBR, these range from **M**5.8 (rupture of segment CS) to **M**7.9 (four-segment rupture of the San Andreas fault). A rupture source probability refers to an earthquake of a specific (characteristic) magnitude occurring on that rupture source. Rupture source probabilities are shown in the lower portion of **Tables 6.4-6.10**. The shaking scenarios discussed in Chapter 7 are for specified rupture sources.

Fault systems. Each of the seven characterized fault systems is host to a variety of rupture sources having a variety of magnitudes (except the single-segment Mt. Diablo thrust, which has only one rupture source). Earthquake probabilities for fault systems are presented in two forms: the chance of occurrence of *any earthquake* on the fault system; and the chance of *earthquakes above a specified magnitude threshold* on the fault system. Both types of fault system probability are shown in the top sections of **Tables 6.4-6.10**, whereas probabilities for earthquakes above given magnitude thresholds are shown in **Table 6.1**.

Background. The background includes all earthquakes in the SFBR other than those occurring on the characterized faults. The probability for the background is specified for earthquakes above a specified threshold. Background probabilities for various magnitude thresholds are shown in **Table 6.1 and 6.11**.

Region. Probabilities of earthquakes in the entire SFBR (or in a sub-region, such as East Bay) combine the probabilities of earthquakes on all of the faults and in the portion of the background included in the region (or sub-region). These are always threshold-type probabilities. Regional probabilities are shown at the bottom of **Table 6.1** and in **Table 6.2**.

Regional Earthquake Probabilities

30-year probabilities of M≥6.7 earthquakes

The probability of one or more large (**M**≥6.7) earthquakes in the SFBR in the next 30 years is 0.62 [0.38 – 0.85] (**Table 6.1, Figure 6.1**). This regional result combines the probabilities of earthquakes on each of the seven characterized fault systems and in the background. The greatest contributors of **M**≥6.7 earthquakes to the regional probability are the Hayward-Rodgers Creek fault system (P=0.27), the San Andreas fault (P=0.21), and the background earthquake sources (P=0.14). The San Gregorio fault (P=0.10) and Calaveras fault (P=0.11) are also significant contributors to the regional probability.

Table 6.1. Probability in 2002-2031 of one or more earthquakes with magnitude **M**6.7 and above, **M**7.0 and above, and **M**7.5 and above, for the characterized fault systems, the background, the SFBR region, and sub-regions east and west of San Francisco Bay. (Region and sub-region values include probability for fault systems and background). The 95% confidence ranges are shown in parentheses.

	M≥6.7	**M**≥7.0	**M**≥7.5
Fault system	Mean [2.5% – 97.5%]	Mean [2.5% – 97.5%]	Mean [2.5% – 97.5%]
San Andreas	0.21 [0.01 – 0.58]	0.17 [0.01 – 0.33]	0.09 [0.01 – 0.18]
Hayward/RC	0.27 [0.10 – 0.58]	0.11 [0.02 – 0.25]	0.00 [0.00 – 0.00]
Calaveras	0.11 [0.03 – 0.27]	0.02 [0.00 – 0.06]	0.00 [0.00 – 0.00]
Concord/GV	0.04 [0.00 – 0.12]	0.00 [0.00 – 0.02]	0.00 [0.00 – 0.00]
San Gregorio	0.10 [0.02 – 0.29]	0.07 [0.01 – 0.20]	0.01 [0.00 – 0.04]
Greenville	0.03 [0.00 – 0.08]	0.01 [0.00 – 0.02]	0.00 [0.00 – 0.00]
Mt Diablo thrust	0.03 [0.00 – 0.08]	0.00 [0.00 – 0.01]	0.00 [0.00 – 0.00]
Background	0.14 [0.07 – 0.37]	0.04 [0.00 – 0.14]	0.00 [0.00 – 0.00]
SF Bay Region	**0.62 [0.38 – 0.85]**	**0.35 [0.17 – 0.56]**	**0.10 [0.02 – 0.19]**

The probabilities for the SFBR as a whole are better constrained than those for any individual fault or for the background. This result follows directly from the average earthquake rates determined by the SFBR earthquake model in Chapter 4. Nevertheless, even the uncertainty in the regional probabilities, from 0.38 to 0.85, is large. The uncertainty in probability reflects uncertainty in the model inputs. How the various sources of uncertainty in the model affect the results presented here is discussed in the **Sensitivities Section** that comes later in this chapter.

The easternmost faults, the Greenville, Concord-Green Valley and Mt. Diablo faults and the northern portion of the Calaveras fault (**Figure 6.2**), have a mean combined probability for **M**≥6.7 earthquakes of 0.19 [0.16 to 0.22].[2] Combining this aggregate probability with the contributions from the Hayward-Rodgers Creek fault, the remaining part of the Calaveras fault, and half the background, we find a probability for **M**≥6.7 earthquakes east and northeast of San Francisco Bay of 0.46 [0.28 to 0.63].

West of San Francisco Bay, the San Andreas and San Gregorio faults have a mean combined probability for a **M**≥6.7 earthquake of 0.29 [0.18 to 0.40]. (**Figure 6.2**). With half of the

[2] Estimates of uncertainty in probability for sub-regions assume that errors in probability on faults are independent and normally distributed.

[3] Probabilities are combined according to Equation 5.9

background probability included, this part of the SFBR has a probability of 0.34 [0.20 to 0.48] for one or more **M**≥6.7 earthquakes in 2002-2031. Thus, the mean probability for **M**≥6.7 earthquakes is greater east of San Francisco Bay than west of it, although the respective confidence bounds substantially overlap. The reverse is the case for **M**≥7.0 earthquakes, however (see next section).

30-year probabilities of larger earthquakes (M≥7.0 and M≥7.5)

The probability of earthquakes on each fault and in the region decreases with increasing earthquake magnitude (**Table 6.1, Figure 6.1**). In the region, the probabilities of M≥7.0 and M≥7.5 earthquakes drop to 0.35 [0.17-0.56] and 0.10 [0.02-0.19], respectively. This decrease is greatest east of San Francisco Bay, where the fault segments are relatively short (20- to 40-km in length) and full-fault ruptures were assessed to be relatively rare. East of San Francisco Bay, the aggregate mean probabilities for **M**≥7.0 and **M**≥7.5 earthquakes are 0.15 and <0.01, respectively. While the faults on this side of the bay have the highest probability of **M**≥6.7 earthquakes, none is capable of generating **M**>7.5 earthquakes, which require rupture lengths of hundreds of kilometers.

West of San Francisco Bay, the longer segments of the San Andreas and San Gregorio faults and the view of the San Andreas source characterization group that the San Andreas fault tends to fail in multi-segment ruptures (Table 6.4) result in a significant production of larger magnitude earthquakes. In this part of the region, the aggregate mean probabilities for **M**≥7.0 and **M**≥7.5 earthquakes are 0.25 and 0.10, respectively.

30-year probabilities of smaller earthquakes (M<6.7).

Smaller earthquakes occurring in urbanized areas may cause significant localized damage. For example, the 1987 **M**5.9 Whittier Narrows earthquake, which occurred in the Los Angeles area, caused $350 million damage, while the larger 1984 **M**6.2 Morgan Hill earthquake, which occurred in a rural region in the southern part of the SFBR, caused $10M damage. However, even smaller earthquakes occurring outside urban areas can have a significant impact; a **M**5.2 earthquake in September 2000, in a rural area 10 miles northwest of the City of Napa resulted in $65 million in damage to that community (California Seismic Safety Commission), *2002, http://www.seismic.ca.gov/sscearth.htm*).

Recent and historical rates of seismicity in the SFBR region can provide plausible bounds on the probability of future (6.0≤**M**<6.7) earthquakes in the region. The most recent 30-year period (1972-2001), in which seismicity appears to be near the minimum of the regional earthquake cycle (**Figure 5.5**), would suggest a 30-year probability of 0.80 for 6.0≤**M**< 6.7 events (equivalently, the expected number N_{exp} of such events is 1.6); this result may serve as a lower bound. In contrast, the most active historical period (1850-1906) would suggest that this probability is 0.99 (N_{exp}=4.6), which may serve as an upper bound for the likelihood of these smaller earthquakes.

The SFBR earthquake model can provide an estimate of the regional probability of smaller earthquakes by assuming a continuous Gutenberg-Richter cumulative magnitude distribution below **M**6.7 with *b*=0.9 (see **Figure 4.5**). This extension of the regional model suggests that, on

average, the probability of 6.0≤**M**<6.7 earthquakes in the SFBR in a 30-year interval is 0.96 [0.91 – 0.99] (N_{exp}=3.3), which lies within the bounds estimated from historical activity.

Which of these estimates is most applicable largely depends on what role the 1906 stress shadow plays in determining the current rate of smaller earthquakes, just as it did in the case of the larger earthquakes. While a formal probability model-weighting procedure was not applied in the calculation of probability of 6.0≤**M**< 6.7 earthquakes, consideration of a stress-shadow effect for these earthquakes would reduce the model result, bringing it closer to the lower bound defined by the more recent seismicity.

Earthquake probabilities at exposure times other than 30 years

The SFBR earthquake model allows us to calculate earthquake probabilities for the region for time intervals other than 30 years (**Figure 6.3**). **Table 6.2** lists SFBR probabilities for 1, 5, 10, 20, and 30 years for both the WG02 weighted, time-dependent model[4] and the long-term average Poisson model. With the Poisson model, we determine an extended regional probability for the next 100 years. **Table 6.2** shows that there is an approximately 50-50 chance of a **M**≥6.7 earthquake in the SFBR in the next 20 years. The similarity in the mean results calculated with the weighted model and the Poisson model over all of the different time periods reflects the distributed weights assigned to the "competing" models—which in turn stems from our uncertainty about the effects of the stress shadow associated with the 1906 earthquake.

Table 6.2. Probability of **M**≥6.7 earthquakes in the SFBR in various exposure times

Exposure Time (years from 2002)	Weighted Models	Poisson Model (Time-independent)
1	0.04 [0.02 - 0.08]	0.03 [0.02 - 0.04]
5	0.16 [0.07 - 0.32]	0.14 [0.11 - 0.18]
10	0.29 [0.14 - 0.49]	0.26 [0.21 - 0.33]
20	0.49 [0.27 - 0.74]	0.46 [0.37 - 0.55]
30	0.62 [0.38 - 0.85]	0.60 [0.51 - 0.70]
100	_	0.96[1] [0.92 - 0.99]

1. Equivalently, the number of **M**≥6.7 earthquakes expected in the SFBR in 100 years is 3.1 [2.4 – 4.1]

Probabilities for Individual Faults and the Background

Earthquake probability in the SFBR is distributed among the seven characterized faults—concentrated more on some than others—as well as in the areas between these faults, which give rise to 'background' earthquakes (**Table 6.1**). On some characterized faults, the probability is unevenly distributed among the segments (**Figure 6.5**, **Table 6.3**). These fault-to-fault and segment-to-segment variations in probability have their origins in the SFBR earthquake model (**Chapter 4)** and in differences among the faults in their slip rates, dates of past earthquakes and interaction effects (**Chapter 5)**.

[4] Estimates for the Empirical Model rate function g(t) were made for the 30-year time interval 2002-2031 (**Table 5.1**). We adopt those estimates here for time intervals shorter than 30 years.

Table 6.3. Probabilities of characterized earthquakes in 2002-2031 on SFBR fault segments

Fault system	Fault segment	Probability											
		All ruptures						**M**≥6.7 ruptures					
		Mean	[	2.5%	–	97.5%	]	Mean	[	2.5%	–	97.5%	]
San Andreas	SAS	0.113	[	0.010	–	0.238	]	0.112	[	0.009	–	0.235	]
	SAP	0.133	[	0.010	–	0.295	]	0.132	[	0.011	–	0.294	]
	SAN	0.116	[	0.014	–	0.235	]	0.114	[	0.013	–	0.233	]
	SAO	0.107	[	0.011	–	0.220	]	0.106	[	0.011	–	0.218	]
Hayward/RC	HS	0.197	[	0.063	–	0.445	]	0.123	[	0.037	–	0.267	]
	HN	0.218	[	0.067	–	0.513	]	0.114	[	0.035	–	0.264	]
	RC	0.177	[	0.053	–	0.460	]	0.170	[	0.052	–	0.430	]
Calaveras	CS	0.316	[	0.050	–	0.640	]	0.023	[	0.000	–	0.098	]
	CC	0.373	[	0.156	–	0.592	]	0.029	[	0.000	–	0.122	]
	CN	0.167	[	0.055	–	0.402	]	0.099	[	0.027	–	0.256	]
Concord/GV	CON	0.140	[	0.027	–	0.359	]	0.031	[	0.000	–	0.110	]
	GVS	0.145	[	0.027	–	0.365	]	0.034	[	0.000	–	0.118	]
	GVN	0.155	[	0.028	–	0.412	]	0.031	[	0.000	–	0.109	]
San Gregorio	SGS	0.056	[	0.009	–	0.154	]	0.054	[	0.008	–	0.140	]
	SGN	0.077	[	0.016	–	0.210	]	0.076	[	0.016	–	0.211	]
Greenville	GS	0.048	[	0.003	–	0.148	]	0.021	[	0.001	–	0.058	]
	GN	0.046	[	0.003	–	0.142	]	0.023	[	0.001	–	0.065	]
Mt Diablo	MTD	0.075	[	0.005	–	0.241	]	0.025	[	0.000	–	0.083	]

In this section we present the earthquake probabilities determined for each fault and for its segments and its rupture sources. We also briefly describe the model characteristics that played a significant role in determining these probabilities. In general, these come down to the slip rate on the fault, choice of fault rupture model, times of previous earthquakes, and the amount of aseismic slip.

San Andreas Fault

The San Andreas fault is the master fault of the SFBR—and all of California—carrying about half of the 36–43 mm/yr plate-motion velocity across the region. As modeled here, it is the only SFBR fault system capable of hosting the largest SFBR earthquakes, such as the four-segment rupture that occurred in 1906. The 470-km-long rupture of the San Andreas fault that occurred in the 1906 earthquake is, by far, the longest surface rupture of any known continental strike-slip earthquake (see **Table 4.2**). The occurrence of such ruptures plays a dominant role in controlling the seismic moment budget in the region. These earthquakes also cast stress shadows of yet unknown duration across the entire Bay region, as was the case following the 1906 earthquake. As noted previously, the nature and duration of this stress shadow are the sources of the greatest uncertainty in the results presented here.

The probability of one or more characterized ruptures occurring on the San Andreas fault in 2002-2031 is 0.24 (**Table 6.4**). Among these, the most likely (in descending order of probability) are a floating rupture (**M**6.90), a full (1906-type) rupture (**M**7.90), a rupture of

segment SAP (**M**7.15), a combined rupture of segments SAS and SAP (**M**7.42), and a combined rupture of segments SAN and SAO (**M**7.70).

The relatively high probability of a floating earthquake reflects three model conditions: the weights applied to the fault–rupture models for the San Andreas fault (Table 3.2); the small magnitude (**M**6.9) relative to the segment ruptures, which allows for a greater frequency of occurrence, and the rate at which the Time–Predictable probability model generates earthquakes of this size. Some support for the floating-earthquake rupture scenario is found in the historical record, with the occurrence of the 1838 **M**6.8 earthquake, which probably, but not certainly, occurred on the San Francisco peninsula segment (SAP) (Bakun, 1999) and with the 1898 **M**6.8 earthquake offshore, near Point Arena, which probably occurred on the San Andreas fault (Ellsworth, 1990; Bakun 2000).

Given the geologic slip rate of the San Andreas fault (17–24 mm/yr), the probabilities for the large magnitude SAS+SAP+SAN+SAO and (SAS+SAP, SAN+SAO) ruptures are primarily fixed by the weighting on the fault-rupture models. The four-segment rupture scenario is supported by the 1906 earthquake and paleoseismic data suggesting even earlier earthquakes rupturing all four segments of the San Andreas fault (Chapter 3). The 2 two-segment rupture probabilities reflect the opinion of the San Andreas SCG that the Golden Gate stepover region is an important segment boundary.

The nearly uniform probabilities for rupture of the four segments that comprise the San Andreas fault in this analysis, ranging from just 0.11 to 0.13, reflects three things: in the BPT model, all four segments were reset in 1906 and the mean recurrence intervals of the segments are similar ranging only from 223 to 229 yr, so the respective phases in the renewal cycles are similar; in the TP model, the distribution of slip in 1906 is similar to the distribution of slip rate on the segments; and in the long-term earthquake model, the floating source, which is the largest contributor of M≥6.7 earthquakes on the fault, is uniformly distributed on the fault.

Despite its status here as a background earthquake, the Loma Prieta earthquake occurred close enough to segment SAS to reduce right-lateral shear stress on this segment, while at the same time providing a loading increment on the adjacent SAP segment. The substantially larger probability for segment SAP (0.044) relative to segment SAS (0.026) mainly reflects the state variable change in the BPT-step and time-predictable models (negative for SAS, positive for SAP) due to that event. Although the choice to treat Loma Prieta as a background earthquake seems significant, its influence on segment SAS through stress transfer is, in fact, nearly as great as it would be if treated as having occurred on that segment. We can compare the case of considering Loma Prieta as a background earthquake (wherein it reduces the failure-readiness of segment SAS through stress transfer), and the case in which Loma Prieta is a rupture of segment SAS (wherein it resets the SAS segment directly in the BPT –step probability method). The probability of an earthquake involving the SAS segment is reduced by less than 25% in the latter case (from 0.10 [0.00–0.27] to 0.08 [0.00–0.16]), a small amount relative to other uncertainties.

Table 6.4. Probabilities for the San Andreas fault, 2002-2031.

San Andreas Fault	Probability
	Mean [2.5% – 97.5%]
Entire Fault system	
All ruptures	0.238 [0.029 – 0.531]
Ruptures M≥6.7	0.235 [0.029 – 0.524]
Ruptures M≥7.0	0.182 [0.015 - 0.379]
Ruptures M≥7.5	0.090 [0.008 - 0.189]
Fault segments - All ruptures	
SAS	0.113 [0.010 – 0.238]
SAP	0.133 [0.010 – 0.295]
SAN	0.116 [0.014 – 0.235]
SAO	0.107 [0.011 – 0.220]
Rupture sources (Mean magnitude)	
SAS (7.03)	0.026 [0.000 – 0.108]
SAP (7.15)	0.044 [0.000 – 0.172]
SAN (7.45)	0.009 [0.000 – 0.037]
SAO (7.29)	0.009 [0.000 – 0.043]
SAS+SAP (7.42)	0.035 [0.001 – 0.102]
SAP+SAN (7.65)	0.000 [0.000 – 0.000]
SAN+SAO (7.70)	0.034 [0.001 – 0.106]
SAS+SAP+SAN (7.76)	0.001 [0.000 – 0.003]
SAP+SAN+SAO (7.83)	0.002 [0.000 – 0.011]
SAS+SAP+SAN+SAO (7.90)	0.047 [0.003 – 0.138]
Floating (6.9)	0.071 [0.004 – 0.264]

Hayward-Rodgers Creek Fault System

The Hayward–Rodgers Creek fault system extends some 140 km, from the Warm Springs district of Fremont, along the east side of San Francisco Bay beneath San Pablo Bay to near Healdsburg on the north. WG90 treated this system as two different and independent faults, the Hayward fault and the Rodgers Creek fault, and for all intents and purposes, so do we, given the low weight assigned to rupture scenarios that involve the Rodgers Creek fault as anything but a single-segment rupture. The geologic slip rate for the three fault segments HS, HN, and RC is 9 ± 2 mm/yr, but on HS and HN a large fraction of the moment rate is expended in aseismic creep.

The Hayward-Rodgers Creek fault system has the highest probability of the characterized faults in SFBR of producing **M**≥6.7 earthquakes in the next 30 years. Its characterized ruptures range in mean magnitude from **M**6.5 to **M**7.3 (**Table 6.5**). The probability of one or more characterized ruptures occurring on the Hayward-Rodgers Creek fault system in 2002-2031 is 0.40, while the corresponding probability for **M**≥6.7 earthquakes is 0.27 (**Table 6.5**). Among the most likely of these (in descending order of probability) are a rupture of segment RC (**M**6.98); a rupture of segment HN (**M**6.49); and a rupture of segment HS (**M**6.67). The high probabilities for these single-segment ruptures reflect the expert-opinion weight placed on such ruptures

(**Table 3.2**) and in the case of RC the relatively long period elapsed since the most recent earthquake. The probability of a M≥7.0 earthquake on the Hayward–Rodgers Creek fault system is relatively low because only two of its rupture sources have mean magnitudes in excess of 7.0 (**Table 6.5**) and both of these have been assigned low weight (**Table 3.2**).

The rupture probabilities for the HS and HN segments illustrate how these probabilities work above and below the **M** ≥ 6.7 threshold. The probability for HN of any type of rupture is 0.218 (**Table 6.5**) and for **M** ≥ 6.7 ruptures is 0.113 (**Table 6.3**), a significant reduction because the mean magnitude of the single-segment rupture is 6.49 and its upper distribution function barely crosses the **M**6.7 threshold (**Figure 6.5**). In addition to a single-segment rupture, the HN segment can rupture in four other ways: HS + HN (0.085 probability), HN + RC (0.018), HS + HN + RC (0.010) and in floating earthquakes apportioned according to length (0.007 x 35km/150km). At these small values, probabilities are additive to a first approximation, and they sum to 0.1146, very close to the **M** ≥ 6.7 probability given above. For **M** ≥ 6.7, then, there is always a minimum rupture probability given approximately by the sum of the probabilities for high-magnitude (**M**>>6.7) ruptures. Such ruptures are represented, for East Bay faults, by multi-segment rupture sources.

The comparable situation for HS is more complicated because the mean magnitude of the single-segment source is **M** = 6.67, essentially the same as the threshold **M** of 6.7. Thus, about half of the single segment-ruptures will have **M** > 6.7 and half will have **M** < 6.7. The probability for HS of any type of rupture is 0.197 (Table 6.5) and for **M** ≥ 6.7 ruptures is 0.123 (Table 6.3). Clearly, the probability of earthquakes can be very sensitive to the threshold level chosen, especially in cases where there are high-probability rupture sources with magnitudes near the threshold of interest.

The principal source of uncertainty in our probability estimates for specific rupture sources on this fault system is the depth extent of aseismic creep on its segments. In our study, we used creep to reduce the source area, and hence magnitude, of potential ruptures. Some data suggest that currently the entire depth extent of the fault creeps aseismically, Another major source of uncertainty is in the position of the HS-HN segmentation point; and, even more fundamentally, in whether the northern extent of the 1868 rupture truly represents an enduring segmentation point at all (i.e., whether the entire Hayward fault always ruptures as a single segment).

Table 6.5. Probabilities for the Hayward-Rodgers Creek fault 2002-2031.

Hayward-Rodgers Creek fault	Probability
	Mean [2.5% – 97.5%]
Entire fault system	
All ruptures	0.397 [0.137 – 0.787]
Ruptures M≥6.7	0.272 [0.096 – 0.578]
Ruptures M≥7.0	0.105 [0.022 - 0.249]
Ruptures M≥7.5	0.000 [0.000 - 0.002]
Fault segments - All ruptures	
HS	0.197 [0.063 – 0.445]
HN	0.218 [0.067 – 0.513]
RC	0.177 [0.053 – 0.460]
Rupture sources (Mean magnitude)	
HS (6.67)	0.113 [0.022 – 0.319]
HN (6.49)	0.123 [0.023 – 0.360]
HS+HN (6.91)	0.085 [0.019 – 0.232]
RC (6.98)	0.152 [0.041 – 0.414]
HN+RC (7.11)	0.018 [0.000 – 0.066]
HS+HN+RC (7.26)	0.010 [0.001 – 0.033]
Floating (6.9)	0.007 [0.003 – 0.016]

Calaveras Fault

The Calaveras fault diverges from the San Andreas fault south of Hollister and extends 123 km in a northerly direction to Danville. The geologic slip rate on the southern two segments (CS and CC) is 15 ± 3 mm/yr, more than a third of the plate motion across the SFBR at these latitudes. North of CC, the Calaveras fault sheds 60% of this slip rate to the Hayward fault, leaving the northern Calaveras fault (CN) with a slip rate of 6 ± 2 mm/yr. Aseismic slip consumes a large fraction of the moment rate expenditure on CS and CC. Paleoseismic data indicate that surface-breaking earthquakes have occurred on segment CN, with the last possibly occurring between 1160 and 1425 AD, but are inconclusive for segments CC and CS. In historical time, the Calaveras fault has been the source of moderate, but not large, earthquakes. The largest of these occurred in 1911 and 1984 (both **M** 6.2) (**Table 2.1**; Bakun, 1999).

Characterized earthquakes on the Calaveras fault range in mean magnitude from **M**5.8 to **M**6.9 (**Table 6.6**). The probability of one of these earthquakes occurring in 2002-2031 is 0.59 [0.024 - 0.90]. Among these, the most likely to occur (in order of descending probability) are a floating earthquake on segment CS or CC (**M**6.2); a rupture of segment CS (**M**5.8); a rupture of segment CC (**M**6.2); and a rupture of segment CN (**M**6.8). Because the characterized ruptures on this fault are moderate in size and segments were judged to rarely link up, the probability of **M**≥6.7 earthquakes here is much lower than it is on the San Andreas or Hayward faults, and the probability of **M**≥7.0 earthquakes is negligible (**Table 6.1**). An increase (from south to north) in

the probability of rupture of a segment of the Calaveras fault (**Table 6.6**) reflects the tapering of aseismic slip assigned to these segments (**Table 4.1**).

Characterizing the long-term earthquake production of the Calaveras fault proved to be extremely challenging. In particular, it is uncertain whether and to what the degree the predominantly creeping segments (CS and CC) are capable of producing large (**M**≥6.7) earthquakes. The high creep rate and repeated historical occurrence of moderate sized earthquakes on these segments suggests that seismic moment release on the Calaveras fault might be largely accommodated by creep and moderate earthquakes. Accordingly, we have placed high weight (0.8) on fault rupture models emphasizing predominantly single-segment and floating **M**6.2 ruptures (**Table 3.5**). Geological evidence to support the existence of segments sufficiently short to host **M**6.2 earthquakes is lacking; therefore, high weight was placed on the floating earthquake source.

Table 6.6 Probabilities for the Calaveras fault, 2002-2031.

Calaveras Fault	Probability
	Mean [2.5% – 97.5%]
Entire fault system	
All ruptures	0.592 [0.243 – 0.895]
Ruptures M≥6.7	0.107 [0.028 – 0.271]
Ruptures M≥7.0	0.015 [0.000 - 0.061]
Ruptures M≥7.5	0.000 [0.000 - 0.000]
Fault segments - All ruptures	
CS	0.316 [0.050 – 0.640]
CC	0.373 [0.156 – 0.592]
CN	0.167 [0.055 – 0.402]
Rupture sources (Mean magnitude)	
CS (5.79)	0.213 [0.000 – 0.538]
CC (6.23)	0.138 [0.039 – 0.297]
CS+CC (6.36)	0.050 [0.000 – 0.203]
CN (6.78)	0.124 [0.030 – 0.356]
CC+CN (6.90)	0.003 [0.000 – 0.036]
CS+CC+CN (6.93)	0.020 [0.000 – 0.079]
Floating (6.2)	0.074 [0.017 – 0.195]
Floating on CS+CC (6.2)	0.251 [0.051 – 0.560]

Concord-Green Valley Fault System

The Concord-Green Valley fault system extends from the vicinity of Walnut Creek north to Wooden Valley, a distance of approximately 56 km (**Figure 3.9**). The Concord-Green Valley fault is believed to carry most of the right lateral slip transferred from the northern Calaveras fault, although this is an area of active investigation. Large earthquakes have not occurred on

either the Concord or the Green Valley faults during the historical period, although a **M**5.4 earthquake occurred on the central part of the Concord fault in 1955 and limited trench observations on both faults indicate the occurrence of ground-breaking ruptures in the past, although the magnitude of those earthquakes is unknown. Aseismic slip at 4-5 mm/yr occurs locally along sections of the Concord-Green Valley fault system and it is not known what portion of the fault system's moment budget is released in large earthquakes. This uncertainty is brought to bear in a large range for the seismic slip factor, *R*, and is a principle contributor the considerable uncertainty in the rupture source magnitudes, recurrence rates, and probabilities.

In our model, characterized earthquakes on the Concord-Green Valley fault range in mean magnitude from **M**6.0 to **M**6.7 (**Table 4.8**). The probability of one of these earthquakes occurring in 2002-2031 is 0.26 [0.04 - 0.60] (**Table 6.7**). Among these, the most likely are a floating earthquake (**M**6.2); a rupture of segment GVN (**M**6.0); a rupture of segment CON (**M**6.3); and a combined rupture of segments CON, GVS and GVN (**M**6.7). Because most of the characterized ruptures on the Concord-Green Valley fault are only moderate in size, the probability of **M**≥6.7 earthquakes here is small and the probability of **M**≥7.0 earthquakes is nil (**Table 6.1)**.

Table 6.7 Probabilities for the Concord-Green Valley fault system, 2002-2031.

Concord-Green Valley Fault	Probability
	Mean [2.5% – 97.5%]
Entire fault system	
All ruptures	0.258 [0.044 – 0.601]
Ruptures M≥6.7	0.036 [0.000 – 0.122]
Ruptures M≥7.0	0.003 [0.000 0.021]
Ruptures M≥7.5	0.000 [0.000 0.000]
Fault segments - all ruptures	
CON	0.140 [0.027 – 0.359]
GVS	0.145 [0.027 – 0.365]
GVN	0.155 [0.028 – 0.412]
Rupture sources (Mean magnitude)	
CON (6.25)	0.050 [0.003 – 0.182]
GVS (6.24)	0.023 [0.001 – 0.087]
CON+GVS (6.58)	0.016 [0.001 – 0.067]
GVN (6.02)	0.061 [0.004 – 0.219]
GVS+GVN (6.48)	0.032 [0.002 – 0.115]
CON+GVS+GVN (6.71)	0.060 [0.007 – 0.222]
Floating (6.2)	0.062 [0.002 – 0.296]

San Gregorio Fault

The San Gregorio fault is a major splay of the San Andreas fault and the westernmost member of the San Andreas Fault system in SFBR. It courses southeastward ~175 km from the Golden

Gate segmentation point along the western edge of the San Francisco Peninsula into and through Monterey Bay (Figure 3.1). Much of the San Gregorio fault is offshore; all of the southern segment of the San Gregorio Fault (SGS) is under water, and more than one active trace is believed to exist beneath Monterey Bay. The past behavior of the San Gregorio fault is known only from paleoseismic investigations on its northern segment (SGN) along the San Mateo County coast, which show the occurrence of large slip events (Simpson and others, 1998). Although the most recent major earthquake probably predates the historical era, there is a small probability that the 1838 earthquake occurred on SGN (Bakun,1999). We cannot rule out the possibility that a rupture source could be formed from the linking of SGN with the San Andreas' SAN segment north of the Golden Gate, but this permutation was not considered likely and was not included in the WG02 segmentation model.

In our model, characterized earthquakes on the San Gregorio fault range in mean magnitude from **M**6.9 (SGS) to **M**7.4 (full rupture) (**Table 6.8**). The probability of one of these earthquakes occurring in 2002-2031 is 0.10 [0.02 - 0.29]. Among these, the most likely is a rupture of segment SGN (**M**7.2). Because its characterized ruptures are relative large in magnitude, owing, in part, to the long length of segment SGN (**Table 4.1**), the San Gregorio fault contributes significantly to the probability of M≥7.0 earthquakes in the SFBR (**Table 6.1**).

Uncertainty in the probabilities estimated for the San Gregorio fault stems from uncertainty about its slip rate, segmentation, and time since the most recent earthquake, as well as our limited ability to model the interaction effects on this fault caused by the 1906 earthquake. Of all the fault segments in the SFBR, segment SGN, being closest to the San Andreas fault, is most strongly affected by the stress redistribution in 1906. It is also perhaps the most challenging segment for modeling the interaction, as the stress change varies rapidly along its length owing to its varying distance from the San Andreas.

Table 6.8 San Gregorio fault probabilities, 2002-2031.

San Gregorio Fault	Probability
	Mean [2.5% – 97.5%]
Entire fault system	
All ruptures	0.104 [0.021 – 0.294]
Ruptures M≥6.7	0.102 [0.021 – 0.285]
Ruptures M≥7.0	0.072 [0.012 - 0.201]
Ruptures M≥7.5	0.009 [0.000 - 0.035]
Fault segments - All ruptures	
SGS	0.056 [0.009 – 0.154]
SGN	0.077 [0.016 – 0.210]
Rupture sources (Mean magnitude)	
SGS (7.0)	0.023 [0.000 – 0.115]
SGN (7.2)	0.039 [0.000 – 0.175]
SGS+SGN (7.4)	0.026 [0.000 – 0.101]
Floating (6.9)	0.021 [0.008 – 0.039]

Greenville Fault

The Greenville fault is the easternmost strand of the San Andreas fault system in SFBR (**Figure 3.1, Figure 3.10**). It extends from the eastern flank of Mt. Diablo south to San Antonio Valley, for a total fault length of 43 ± 20 km. The central Greenville fault produced **M**5.8 and **M**5.4 earthquakes in 1980 (Bolt *et al.*,1981). Current paleoseismic data indicate that surface faulting earthquakes have occurred in the past, but their magnitudes are unknown.

In our model, characterized earthquakes on the Greenville fault range in mean magnitude from **M**6.2 (GN) to **M**6.9 (full rupture) (**Table 6.9**). The probability of one of these earthquakes occurring in 2002-2031 is 0.08 [0.01 - 0.22]. Among these, the most likely are ruptures of segment GS (**M**6.6) and segment GN (**M**6.7). The probability of a one or more **M**≥6.7 earthquakes occurring in 2002-2031 on the Greenville fault is 0.03 (**Table 6.1**). The uncertainties on these numbers are large, due to the lack of information indicating whether the fault's northern and southern segments tend to rupture together or separately (**Table 3.7**).

Table 6.9 Greenville fault probabilities, 2002–2031.

Greenville Fault	Probability
	Mean [2.5% – 97.5%]
Entire fault system	
All ruptures	0.077 [0.007 – 0.222]
Ruptures M≥6.7	0.030 [0.002 – 0.082]
Ruptures M≥7.0	0.005 [0.000 - 0.016]
Ruptures M≥7.5	0.000 [0.000 - 0.000]
Fault segments - All ruptures	
GS	0.048 [0.003 – 0.148]
GN	0.046 [0.003 – 0.142]
Rupture sources (Mean magnitude)	
GS (6.6)	0.031 [0.000 – 0.107]
GN (6.7)	0.029 [0.000 – 0.098]
GS+GN (6.9)	0.015 [0.001 – 0.047]
Floating (6.2)	0.004 [0.001 – 0.009]

Mount Diablo Thrust Fault

The Mt. Diablo thrust a blind fault, one not directly observable at the Earth's surface **(Figure 3.1, Figure3.10)**. Blind thrust faults elsewhere in California have hosted produced damaging earthquakes, including the 1983 Coalinga, 1989 Loma Prieta, and 1994 Northridge events. The fault itself, its geometry, and rates of slip are inferred from structural and kinematic models. The Unruh and Sawyer (1997) interpretation, adopted herein, is that the blind thrust is a manifestation of crustal shortening within a fold-and-thrust belt, driven by a restraining transfer of slip from the Greenville fault to the Concord fault. The Mt. Diablo thrust fault is thought to underlie the asymmetric, southwest-vergent Mt. Diablo and Tassajara anticlines for a total length of 25 ± 5

km (Crane, 1995; Unruh and Sawyer, 1997). There is no basis for segmenting the fault, and it is treated as a single earthquake source.

In our model, the single-segment Mt. Diablo fault produces earthquakes with mean magnitude **M**6.65. The probability of one of these earthquakes occurring in 2002-2031 is 0.08 [0.01 - 0.24] (**Tables 6.1, 6.10**); the corresponding probability for **M**≥6.7 earthquakes is 0.03.

Table 6.10 Mt. Diablo fault probabilities, 2002–2031.

Mt Diablo Fault	Probability
	Mean [2.5% – 97.5%]
Single-segment fault (mean magnitude 6.65)	
All ruptures	0.075 [0.005 – 0.241]
Ruptures M≥6.7	0.025 [0.000 – 0.083]

Background earthquakes

While the seven faults characterized in the SFBR earthquake model are the most important and best understood faults in the region, other faults contribute to the earthquake probability in the region as well. These include faults for which we lack sufficient information for characterization in the model and faults that slip rates less than 1 mm/yr. In addition to these are (presumably) other faults in the region that are yet to be discovered. The Loma Prieta earthquake is classified as a background event. All the uncharacterized faults and unknown faults in the SFBR constitute the background.

The Thrust and Reverse SCG reviewed geodetic data, geologic data, and global plate motion models that provide constraints on rates of deformation across the boundary between the Pacific plate and the Sierra Nevada-Great Valley microplate. They identified several subregions (or "hot spots") within SFBR characterized by significant contractional strain rates accommodated by numerous thrust faults with low slip rates. Among the thrust faults currently mapped within these zones, only the Mt. Diablo thrust was assigned a slip rate exceeding 1 mm/yr and was therefore treated as a characterized fault.

An analysis by Wesson and others [2002] of historical earthquakes in the SFBR used probabilistic methods to associate known events with either one of the18 characterized fault segments or with an uncharacterized source fault. This analysis shows that a significant fraction of the historical events occurred on uncharacterized faults and that these earthquakes (and faults) released a significant fraction of the seismic moment within the SFBR (**Figure 2.6**).

As discussed in **Chapter 5**, we modeled the background differently from the characterized faults. We used a truncated Gutenberg-Richter model (with maximum magnitude **M**7.25 [7.0 - 7.5]) fit to historical earthquake occurrence, together with the Poisson probability model.

The probability of a **M**≥6.7 earthquake occurring in 2002-2031 on a fault in the background is 0.14 [0.07 – 0.37] (**Table 6.11**). This probability is a substantial part of the regional earthquake probability, exceeded only by the corresponding probabilities on the San Andreas and Hayward-Rodgers Creek faults (**Table 6.1**). Thus the uncharacterized faults contribute significantly to the regional probability in the SFBR and "fill in" the areas between the characterized faults as possible sites of large earthquakes.

Table 6.11. Probabilities for background earthquakes, 2002–2031.

Magnitude	Probability Mean [2.5% – 97.5%]
M≥6.0	0.56 [0.40 – 0.93]
M≥6.5	0.23 [0.14 – 0.55]
M≥6.7	0.14 [0.07 – 0.37]
M≥7.0	0.04 [0.00 – 0.14]
M≥7.5	0.00 [0.00 – 0.00]

Comparison of Results to Earlier Probability Reports

Previous assessments of earthquake probabilities in the SFBR were made in 1988 (WG88) and1990 (WG90). Those Working Groups focused on the most active faults, and estimated earthquake probability only for those with sufficient data for time-predictable probability calculations. Both reports used a nominal magnitude threshold of **M**≥7. WG88 analyzed the San Andreas fault and Hayward fault, and concluded that the 30-year probability (1988 to 2018) of earthquakes on each fault was 0.5. They also assigned an average to low level of reliability to the individual probabilities for the most important sources (which roughly correspond to our single-segment rupture sources SAS, SAP, HS, HN).

WG90 included the Rodgers Creek fault in its assessment, and introduced the use of a logic tree for the calculation sequence. Like WG88, they relied exclusively on the time-predictable probability model. Their regional probability of **M**≥7 earthquakes (1990 to 2020) was 0.67, with the Hayward-Rodgers Creek fault system the principal contributor to the probability. On the San Andreas fault, their Peninsula segment had the highest probability.

An innovation introduced in the SCEC Phase II report—and also used by WG99 and in this study—is the inclusion of an overall moment budget, taken as the geodetically determined strain accumulation across the breadth of the region of 36 to 43 mm/yr. This constraint assured that the long-term SFBR model would agree with both geodetic and plate motion rates (**Figure 6.6**). Another innovation is the use of alternative probability models that differ, most importantly, in their treatment of the 1906 "stress-shadow" in the San Francisco Bay region.

Qualitatively, our results agree with these those of WG90: the fault segments most likely to rupture in **M**≥6.7 earthquakes in the SFBR are the Hayward-Rodgers Creek fault and the Peninsula segment of the San Andreas fault (**Table 6.3)**. However, there are significant differences (relative to WG90) for the Hayward fault and the Peninsula segment of the San Andreas fault, where we calculate lower probabilities. These differences have origins in three

areas: the inclusion of new and better data (specifically, a new interpretation of the 1838 earthquake by Toppozada and Borcherdt, 1998); the accounting for the effects of the 1906 and 1989 stress changes (stress shadows); and the inclusion of aseismic slip (creep) on—and the shortening of—some segments in our fault model (e.g., HN).

By extending the analysis of earthquake probability to five additional faults and including earthquake sources in the "background", we are able to present a broader regional perspective than WG90 did—one in which earthquake potential is more dispersed throughout the SFBR (**Figure 6.6**).

Differences in fault model

We built on (and only modified where necessary) earlier segmentation models established by the1996 Working Group on Northern California Earthquake Potential (WGNCEP96). On the San Andreas fault, we changed the segmentation of the San Andreas by moving the northern boundary of the Peninsula segment (SAP) to the Golden Gate and changed its slip rate (increasing it north of the Golden Gate from 19 to 24 mm/year and decreasing it to the south from 19 to 17 mm/yr). We increased the length of the Santa Cruz segment (SAS) to 62 km, relative to the 35 km, 39 km, and 37 km lengths defined by WG88, WG90, and WGNCEP96, respectively.

For the Hayward-Rodgers Creek fault, we adopted the slip rate used in WG90. We retained the three-segment fault system, but increased the length of HS and decreased the length of HN, based on Yu and Segall's (1996) reinterpretation of the length of the 1868 rupture.

Other important differences relative to the WG90 study include our use of alternative rupture scenarios (involving single-segment and multi-segment ruptures); assignment of earthquake magnitudes based on rupture area; and introduction of the R factor (used to account for aseismic slip or creep on characterized faults). These factors affect both the calculation of both magnitudes and mean recurrence intervals and therefore probability.

Some of the effects of these differences can be seen in **Table 6.12,** which compares the WG90 and WG02 models for segments of the San Andreas and Hayward-Rodgers Creek faults and shows the resulting estimated mean recurrence intervals for segment ruptures. On the Hayward-Rodgers Creek fault, model changes resulted in negligible changes in calculated mean recurrence interval. However, on the San Andreas fault these changes had a larger effect, particularly on segments SAP and SAS, where a decrease in loading rate and increase in segment length lead to significantly longer recurrence times.

Table 6.12 Comparison of fault parameters in WG90 and WG02.

Segment	Slip Rate (mm/yr)		Segment Length (km)		Mean Recurrence Interval[1] (yr)		Displacement (m)	Reliability
	WG90	**WG02**	WG90	**WG02**	WG90	**WG02**	WG90	WG90
SAO	—	**24±3**	—	**145±11**	—	**225**	—	—
SAN	19±4	**24±3**	340±5	**182±11**	228	**223**	4.5±0.5	B
SAP	19±4	**17±4**	61±5	**85±13**	136	**229**	2.6	C
SAS	19±4	**17±4**	39±5	**61±15**	91	**224**	1.8	C
RC	9±2	**9±2**	50±5	**63±10**	≥222	**205**	2.0±0.5	C
HN	9±2	**9±2**	50±7.5	**30±15**	167	**155**	1.5±0.5	D
HS	9±2	**9±2**	32±7.5	**55±19**	167	**161**	1.5±0.5	D

1. Recurrence intervals correspond to earthquakes of differing magnitude.

Differences in probability modeling, including treatment of stress effects from the 1906 earthquake

We broke the tradition of previous working groups by not adopting a single probability model for our calculations. We took this approach because no single probability model known to us appears to be fully satisfactory in representing the effect of the 1906 stress shadow – an effect that likely plays a major role in defining the probabilities. We applied the time-predictable model only to the San Andreas fault because the information available for the remainder of the SFBR faults was either lacking or judged to be too uncertain.

WG88 and WG90 used a *qualitative* scale (A-E, with A being the most reliable) to rate its confidence in the segment probabilities. We attempted to quantify uncertainty in all parts of our model, from basic geologic observations to modeled stress interaction effects, and explicitly carried these uncertainties through the calculation. This method provides a *quantitative* description of the uncertainty in the probabilities.

WG90 did not consider the effect on adjacent faults of stress changes associated with the 1906 earthquake. In our calculations, the stress changes in 1906 reduced the regional probability – in some probability models greatly, in others to a lesser degree. As we have discussed in **Chapter 5**, and will discuss further in the sensitivity analysis presented later in this chapter, these stress shadow effects produce the greatest single contribution to the reduction in the regional probability of earthquakes determined in this study, relative to that in WG90. The wide range of probability calculated with our probability models is indicative of our limited understanding of the fundamental physics of stress interaction processes.

The introduction of the new Brownian Passage Time probability model (BPT) allowed us to apply the stress changes produced by the 1906 earthquake directly in the probability calculation through a formal “state change”, rather than through a “clock correction,” as was done in WG90 and WG99. On fault segments relatively close to failure (e.g., segments RC and HS), the resulting changes in the calculated probabilities are transient and characteristically decay with

elapse time following the stress step (**Figure 5.9**). On segments earlier in the recurrence cycle, the BPT and clock change methods produce probability changes that are similar to each other. Other than in their response to a sudden stress change, the BPT and Lognormal probability models produce very similar results (**Table 6.13**), as expected, considering the similarity of their pdf's (**Figure 5.3**).

Table 6.13 Comparison of probability calculations made with Lognormal and BPT models without fault interactions.

Fault	Probability of M≥6.7 Earthquake in 2002-2031	
	Lognormal Model	BPT Model
San Andreas	0.172	0.176
Hayward-Rodgers Creek	0.381	0.377
Calaveras	0.161	0.160
Concord Green Valley	0.051	0.051
San Gregorio	0.148	0.148
Greenville	0.040	0.040
Mt. Diablo	0.038	0.038
Region (not including background)	0.679	0.678

We calculated the long-term probabilities for smaller (6≤**M**<6.7) earthquakes (in the region (based on observed regional seismicity and the use of a truncated Gutenberg-Richter model and the Poisson probability model). WG90 did not consider earthquakes smaller than the characteristic earthquakes, which had "nominal" magnitude ~**M**7.

Differences in presentation of results

The interest in WG90 was in "large earthquakes," which simply meant earthquakes with expected magnitude **M**~7 (or, on the north coast segment of the San Andreas fault, **M**~8). Other than by providing a length for the Hayward-Rodgers Creek fault displacement estimates, the segment lengths measured in WG90 did not enter into the probability calculations. In contrast, our model allows for a variety of possible ruptures that span a range of magnitude from **M**6.2 to **M**7.9. This feature allows us to calculate probabilities for various magnitude thresholds. A consequence of this change is seen in the case of the northern Hayward fault (segment HN), where we model the mean magnitude for a rupture of this segment by itself to be **M**6.5 (**Table 6.5**). The probability calculated for this rupture depends on the magnitude threshold (**Table 6.3**). To meaningfully compare our result for segment HN to that of WG90, we disregard the difference in the respective magnitudes for events on this segment and use our segment probability for all ruptures (**Table 6.3**; **Table 6.14**). On the Hayward-Rodgers Creek fault, the WG90 probabilities for each segment fall approximately midway between comparable WG02 calculations made with and without considering the effect of the 1906 stress changes.

Table 6.14. Comparison of segment rupture probabilities in WG90 and WG02

Fault Segment	WG90 Probability of a characteristic earthquake on fault segment	WG02 Probability of a characterized earthquake of any size on fault segment. Mean [95% confidence range]	
		BPT (no step)	Weighted Models
HS	0.23	0.29 [0.13 - 0.56]	0.21 [0.07 - 0.48]
HN	0.28	0.32 [0.16 - 0.56]	0.23 [0.07 - 0.53]
RC	0.22	0.28 [0.13 - 0.56]	0.19 [0.06 - 0.49]
SAP	0.23	0.12 [0.06 - 0.25]	0.14 [0.02 - 0.29]
H/RC fault	0.57	0.56 [0.31 - 0.87]	0.42 [0.15 - 0.81]

WG90's probability for SAP is significantly higher than ours, lying only barely within our 95% confidence bound. This difference stems from differences in the fault models. We extended the northern end of SAP north to the Golden Gate, making its length 85 km, compared to 61 km in the WG90 model. We modeled the single-segment rupture of SAP with mean magnitude 7.17, compared to 7 in WG90. And we used a slightly lower slip rate than did WG90. As a result of these differences, our mean recurrence interval for SAP is greater (**Table 6.12**) and probability lower (**Table 6.14**).

Sensitivity of the Results to Modeling Assumptions and Parameter Uncertainties

The calculations presented are the most complex and comprehensive analysis of earthquake hazard in the region to date, increasing (over the WG90 model) the number of characterized faults from 3 to 7 and the number of modeled fault segments from 6 to 18, and expanding the branching structure of the calculation sequence to include multiple fault rupture and earthquake probability models. The alternatives and weights defining the branching structure represent uncertainty about virtually all aspects of the model, including the geometry, slip rate, and segmentation of the faults, the relationship between source rupture area and earthquake magnitude, and the effect of aseismic slip.

From the outset, a guiding philosophy in our work has been that all sources of uncertainty about the earthquake process in the SFBR should be represented in the model. This approach acknowledges our incomplete knowledge about both the long term behavior of the earthquake machine in the SFBR and its current state as regards the probability for large earthquakes in the next 30 years. We felt that through such an approach, new information, as it became available in the future, could easily be incorporated by either eliminating branches in the calculation sequence or better constraining model parameter values. The comprehensive quantification of uncertainty about the earthquake process in the SFBR was one of the primary scientific goals of the Working Group—to be developed in parallel with the estimation of the current 30-year probabilities of earthquakes in the region.

The principal sources of uncertainty recognized in this study were introduced in **Chapter 4**. Here, we explore how these uncertainties affect the estimates of the 30-year probability of

earthquakes. While all sources of uncertainty have some influence on the probability calculations, the results are particularly sensitive to a small number of key inputs and modeling choices. The remainder of this section includes a series of sensitivity analyses for these key factors, which help put the calculations into context in two ways. First, they illustrate how well (or poorly) our knowledge constrains the estimated probabilities. Beyond that, sensitivity analyses can identify those research areas in which discovery of new information may be most valuable for sharpening future estimates of earthquake probabilities in the SFBR, which is the subject of **Chapter 8**.

Choice of probability model and treatment of post-1906 seismic quiescence

As discussed in **Chapter 5**, a major source of uncertainty in the 30-year probability estimates arises in quantifying the effects of the 1906 stress shadow. We took two approaches toward incorporating the post-1906 regional quiescence in our probability calculations. The first approach uses estimates of 1906 stress changes and long-term loading rates calculated from elastic dislocation models to adjust the state of the Brownian Passage Time model in 1906. As discussed in **Chapter 5,** the elastic models seem to underestimate the duration of the stress shadow and suggest that most faults are no longer in the stress shadow. As a result, the regional 30-year probability in 2002 calculated using this approach is considered to be an upper bound.

In the second approach, the Empirical model extrapolated relative rates of seismicity in the later half of the 20th century as a proxies for the effect of fault interaction. This model suggests that most of the faults remain in the stress shadow; it produces lower 30-year probabilities, which we consider to be a likely lower bound.

We also considered two models that ignore 1906 effects altogether: a Poisson probability model, and a BPT model without fault interactions. Finally, for the San Andreas fault only, a time-predictable model used information about the amount of slip that occurred in 1906. We placed significant weight on each of these approaches in the calculation sequence (**Table 5.4**, **Figure 5.10**). The absence of a single probability model that was strongly favored among the working group members indicates the widely disparate views currently held in this crucial area and underscores the need for better physical models for fault interaction in future efforts to estimate earthquake probability.

The results in **Table 6.1** for the characterized faults and the region come from our preferred model, which is a weighted combination of i the 5 probability models considered. Probabilities calculated using each of the individual probability models for the occurrence of M≥6.7 earthquakes in the region and on the characterized faults are listed in **Table 6.15**. Corresponding probabilities for M≥6.7 earthquakes involving individual fault segments and rupture sources are listed in **Tables 6.16** and **6.17**, respectively.

Table 6.15. Probabilities for the occurrence of **M**≥6.7 earthquakes occurring on characterized faults in 2002-2031, calculated with individual probability models and with the weighted set of probability models. Probabilities for the background are always calculated with the Poisson model. Probabilities for the region combine those for the characterized faults and the background. (Note: In this table, aggregate probabilities for the SF Bay Region and the San Andreas fault include contributions from characterized earthquakes outside the SFBR "box", specifically single-segment ruptures of segment SAO and floating earthquakes on the northern extent of the San Andreas fault.)

	Weighted results						Poisson						Empirical						BPT (renewal)						BPT + stress step						Time-predictable					
Fault system	Mean	[	2.5%	–	97.5%	]	Mean	[	2.5%	–	97.5%	]	Mean	[	2.5%	–	97.5%	]	Mean	[	2.5%	–	97.5%	]	Mean	[	2.5%	–	97.5%	]	Mean	[	2.5%	–	97.5%	]
San Andreas	0.235	[	0.029	–	0.524	]	0.196	[	0.113	–	0.299	]	0.118	[	0.059	–	0.195	]	0.176	[	0.018	–	0.368	]	0.166	[	0.017	–	0.374	]	0.385	[	0.117	–	0.562	]
Hayward/Rodgers Cr	0.272	[	0.096	–	0.578	]	0.227	[	0.161	–	0.304	]	0.138	[	0.084	–	0.200	]	0.377	[	0.220	–	0.650	]	0.342	[	0.194	–	0.610	]	-					
Calaveras	0.107	[	0.028	–	0.271	]	0.093	[	0.036	–	0.180	]	0.055	[	0.020	–	0.111	]	0.160	[	0.055	–	0.327	]	0.150	[	0.050	–	0.315	]	-					
Concord/Green Valley	0.036	[	0.000	–	0.122	]	0.032	[	0.000	–	0.082	]	0.018	[	0.000	–	0.050	]	0.051	[	0.000	–	0.151	]	0.048	[	0.000	–	0.145	]	-					
San Gregorio	0.102	[	0.021	–	0.285	]	0.097	[	0.036	–	0.181	]	0.057	[	0.020	–	0.114	]	0.148	[	0.020	–	0.376	]	0.124	[	0.018	–	0.316	]	-					
Greenville	0.030	[	0.002	–	0.082	]	0.031	[	0.011	–	0.055	]	0.018	[	0.006	–	0.033	]	0.040	[	0.000	–	0.111	]	0.036	[	0.000	–	0.100	]	-					
Mt Diablo thrust	0.025	[	0.000	–	0.083	]	0.026	[	0.000	–	0.070	]	0.015	[	0.000	–	0.040	]	0.038	[	0.000	–	0.129	]	0.038	[	0.000	–	0.127	]	-					
Background (other sources)	0.139	[	0.069	–	0.365	]	0.139	[	0.069	–	0.365	]	0.139	[	0.069	–	0.365	]	0.139	[	0.069	–	0.365	]	0.139	[	0.069	–	0.365	]	-					
SF Bay Region	0.633	[	0.377	–	0.879	]	0.600	[	0.508	–	0.701	]	0.445	[	0.324	–	0.579	]	0.720	[	0.584	–	0.893	]	0.687	[	0.544	–	0.868	]	-					

Table 6.16. Probabilities that each fault segment will rupture in a **M**≥6.7 earthquakes in 2002-2031, calculated with individual probability models and with the weighted set of probability models.

		Weighted results					Poisson					Empirical					BPT (renewal)					BPT + stress step					Time-predictable				
Fault system	Segment	Mean	[	2.5%	–	97.5%	]	Mean	[	2.5%	–	97.5%	]	Mean	[	2.5%	–	97.5%	]	Mean	[	2.5%	–	97.5%	]	Mean	[	2.5%	–	97.5%	]	Mean	[	2.5%	–	97.5%	]
San Andr.	SAS	0.112	[	0.009	–	0.234	]	0.124	[	0.078	–	0.173	]	0.073	[	0.040	–	0.112	]	0.110	[	0.004	–	0.228	]	0.099	[	0.004	–	0.272	]	0.139	[	0.037	–	0.236	]
	SAP	0.131	[	0.010	–	0.290	]	0.121	[	0.075	–	0.170	]	0.072	[	0.039	–	0.110	]	0.108	[	0.004	–	0.223	]	0.100	[	0.005	–	0.233	]	0.198	[	0.057	–	0.327	]
	SAN	0.116	[	0.014	–	0.235	]	0.125	[	0.072	–	0.178	]	0.074	[	0.038	–	0.115	]	0.114	[	0.009	–	0.233	]	0.111	[	0.009	–	0.231	]	0.140	[	0.026	–	0.257	]
	SAO	0.107	[	0.011	–	0.220	]	0.124	[	0.071	–	0.176	]	0.073	[	0.038	–	0.115	]	0.112	[	0.007	–	0.233	]	0.109	[	0.007	–	0.232	]	0.116	[	0.020	–	0.219	]
Hayward/RC	HS	0.123	[	0.036	–	0.266	]	0.107	[	0.051	–	0.160	]	0.063	[	0.028	–	0.102	]	0.171	[	0.073	–	0.319	]	0.153	[	0.063	–	0.284	]	-					
	HN	0.113	[	0.034	–	0.264	]	0.093	[	0.054	–	0.139	]	0.054	[	0.028	–	0.086	]	0.159	[	0.076	–	0.315	]	0.144	[	0.068	–	0.282	]	-					
	RC	0.170	[	0.053	–	0.431	]	0.131	[	0.083	–	0.181	]	0.078	[	0.043	–	0.122	]	0.248	[	0.122	–	0.512	]	0.221	[	0.102	–	0.473	]	-					
Calaveras	CS	0.023	[	0.000	–	0.098	]	0.022	[	0.000	–	0.087	]	0.013	[	0.000	–	0.052	]	0.032	[	0.000	–	0.118	]	0.031	[	0.000	–	0.115	]	-					
	CC	0.029	[	0.000	–	0.122	]	0.030	[	0.000	–	0.119	]	0.017	[	0.000	–	0.071	]	0.041	[	0.000	–	0.144	]	0.039	[	0.000	–	0.141	]	-					
	CN	0.099	[	0.027	–	0.256	]	0.084	[	0.036	–	0.128	]	0.049	[	0.020	–	0.080	]	0.151	[	0.054	–	0.310	]	0.141	[	0.048	–	0.294	]	-					
Concord/GV	CON	0.031	[	0.000	–	0.110	]	0.028	[	0.000	–	0.078	]	0.016	[	0.000	–	0.048	]	0.045	[	0.000	–	0.140	]	0.042	[	0.000	–	0.133	]	-					
	GVS	0.034	[	0.000	–	0.118	]	0.030	[	0.000	–	0.081	]	0.018	[	0.000	–	0.049	]	0.049	[	0.000	–	0.148	]	0.046	[	0.000	–	0.142	]	-					
	GVN	0.031	[	0.000	–	0.109	]	0.027	[	0.000	–	0.078	]	0.016	[	0.000	–	0.047	]	0.044	[	0.000	–	0.141	]	0.041	[	0.000	–	0.134	]	-					
San Gregor.	SGS	0.050	[	0.005	–	0.136	]	0.048	[	0.015	–	0.074	]	0.028	[	0.009	–	0.045	]	0.072	[	0.003	–	0.196	]	0.063	[	0.003	–	0.175	]	-					
	SGN	0.080	[	0.018	–	0.216	]	0.076	[	0.034	–	0.127	]	0.044	[	0.019	–	0.078	]	0.121	[	0.017	–	0.305	]	0.097	[	0.015	–	0.247	]	-					
Greenville	GS	0.021	[	0.001	–	0.058	]	0.021	[	0.008	–	0.037	]	0.012	[	0.004	–	0.022	]	0.028	[	0.000	–	0.081	]	0.025	[	0.000	–	0.073	]	-					
	GN	0.023	[	0.001	–	0.065	]	0.024	[	0.009	–	0.041	]	0.014	[	0.005	–	0.025	]	0.031	[	0.000	–	0.091	]	0.028	[	0.000	–	0.082	]	-					
Mt Diablo	MTD	0.025	[	0.000	–	0.083	]	0.026	[	0.000	–	0.070	]	0.015	[	0.000	–	0.040	]	0.038	[	0.000	–	0.129	]	0.038	[	0.000	–	0.127	]	-					

Table 6.17. Probabilities that each rupture source will fail in a **M**≥6.7 earthquake in 2002-2031, calculated with individual probability models and with the weighted set of probability models.

		Weighted results						Poisson						Empirical						BPT (renewal)						BPT + stress step						Time-predictable					
Fault system	Rupture source	Mean	[	2.5%	–	97.5%	]	Mean	[	2.5%	–	97.5%	]	Mean	[	2.5%	–	97.5%	]	Mean	[	2.5%	–	97.5%	]	Mean	[	2.5%	–	97.5%	]	Mean	[	2.5%	–	97.5%	]
San Andr.	SAS	0.025	[	0.000	–	0.105	]	0.021	[	0.000	–	0.044	]	0.012	[	0.000	–	0.027	]	0.018	[	0.000	–	0.056	]	0.013	[	0.000	–	0.104	]	0.047	[	0.002	–	0.126	]
	SAP	0.043	[	0.000	–	0.171	]	0.015	[	0.000	–	0.030	]	0.008	[	0.000	–	0.018	]	0.013	[	0.000	–	0.037	]	0.011	[	0.000	–	0.038	]	0.108	[	0.023	–	0.204	]
	SAN	0.009	[	0.000	–	0.037	]	0.004	[	0.000	–	0.022	]	0.002	[	0.000	–	0.014	]	0.004	[	0.000	–	0.029	]	0.004	[	0.000	–	0.029	]	0.020	[	0.001	–	0.046	]
	SAO	0.009	[	0.000	–	0.043	]	0.007	[	0.000	–	0.033	]	0.004	[	0.000	–	0.020	]	0.006	[	0.000	–	0.042	]	0.006	[	0.000	–	0.042	]	0.015	[	0.000	–	0.053	]
	SAS+SAP	0.035	[	0.001	–	0.102	]	0.028	[	0.006	–	0.083	]	0.016	[	0.003	–	0.051	]	0.025	[	0.000	–	0.108	]	0.021	[	0.000	–	0.116	]	0.061	[	0.015	–	0.106	]
	SAP+SAN	0.000	[	0.000	–	0.000	]	0.000	[	0.000	–	0.000	]	0.000	[	0.000	–	0.000	]	0.000	[	0.000	–	0.000	]	0.000	[	0.000	–	0.000	]	0.000	[	0.000	–	0.000	]
	SAN+SAO	0.034	[	0.001	–	0.106	]	0.035	[	0.011	–	0.100	]	0.021	[	0.006	–	0.058	]	0.033	[	0.000	–	0.131	]	0.033	[	0.000	–	0.131	]	0.040	[	0.002	–	0.083	]
	SAS+SAP+SAN	0.001	[	0.000	–	0.003	]	0.001	[	0.000	–	0.004	]	0.000	[	0.000	–	0.002	]	0.001	[	0.000	–	0.005	]	0.001	[	0.000	–	0.004	]	0.001	[	0.000	–	0.001	]
	SAP+SAN+SAO	0.002	[	0.000	–	0.011	]	0.002	[	0.000	–	0.011	]	0.001	[	0.000	–	0.007	]	0.002	[	0.000	–	0.013	]	0.002	[	0.000	–	0.013	]	0.001	[	0.000	–	0.002	]
	SAS+SAP+SAN+SAO	0.047	[	0.003	–	0.138	]	0.076	[	0.036	–	0.119	]	0.045	[	0.019	–	0.077	]	0.068	[	0.001	–	0.156	]	0.065	[	0.001	–	0.154	]	0.019	[	0.004	–	0.033	]
	floating M6.9	0.068	[	0.004	–	0.253	]	0.025	[	0.004	–	0.052	]	0.015	[	0.002	–	0.031	]	0.025	[	0.004	–	0.052	]	0.025	[	0.004	–	0.052	]	0.159	[	0.033	–	0.286	]
Hayward/RC	HS	0.043	[	0.000	–	0.133	]	0.039	[	0.000	–	0.099	]	0.023	[	0.000	–	0.060	]	0.059	[	0.000	–	0.166	]	0.052	[	0.000	–	0.151	]	–					
	HN	0.015	[	0.000	–	0.089	]	0.011	[	0.000	–	0.057	]	0.006	[	0.000	–	0.032	]	0.021	[	0.000	–	0.110	]	0.019	[	0.000	–	0.099	]	–					
	HS+HN	0.072	[	0.017	–	0.189	]	0.060	[	0.025	–	0.109	]	0.035	[	0.013	–	0.067	]	0.103	[	0.034	–	0.230	]	0.093	[	0.031	–	0.205	]	–					
	RC	0.144	[	0.041	–	0.384	]	0.107	[	0.065	–	0.157	]	0.063	[	0.034	–	0.102	]	0.213	[	0.099	–	0.463	]	0.188	[	0.080	–	0.430	]	–					
	HN+RC	0.018	[	0.000	–	0.065	]	0.014	[	0.000	–	0.038	]	0.008	[	0.000	–	0.023	]	0.027	[	0.000	–	0.079	]	0.024	[	0.000	–	0.072	]	–					
	HS+HN+RC	0.010	[	0.001	–	0.033	]	0.008	[	0.002	–	0.020	]	0.005	[	0.001	–	0.012	]	0.015	[	0.002	–	0.040	]	0.013	[	0.002	–	0.036	]	–					
	floating M6.9	0.007	[	0.003	–	0.015	]	0.008	[	0.004	–	0.016	]	0.005	[	0.002	–	0.010	]	0.008	[	0.004	–	0.016	]	0.008	[	0.004	–	0.016	]	–					
Calaveras	CS	0.000	[	0.000	–	0.000	]	0.000	[	0.000	–	0.000	]	0.000	[	0.000	–	0.000	]	0.000	[	0.000	–	0.000	]	0.000	[	0.000	–	0.000	]	–					
	CC	0.005	[	0.000	–	0.048	]	0.005	[	0.000	–	0.056	]	0.003	[	0.000	–	0.032	]	0.005	[	0.000	–	0.061	]	0.005	[	0.000	–	0.060	]	–					
	CS+CC	0.005	[	0.000	–	0.049	]	0.005	[	0.000	–	0.053	]	0.003	[	0.000	–	0.031	]	0.006	[	0.000	–	0.058	]	0.006	[	0.000	–	0.057	]	–					
	CN	0.080	[	0.018	–	0.225	]	0.065	[	0.023	–	0.108	]	0.038	[	0.012	–	0.067	]	0.124	[	0.036	–	0.282	]	0.115	[	0.032	–	0.264	]	–					
	CC+CN	0.002	[	0.000	–	0.033	]	0.002	[	0.000	–	0.028	]	0.001	[	0.000	–	0.017	]	0.004	[	0.000	–	0.045	]	0.003	[	0.000	–	0.043	]	–					
	CS+CC+CN	0.018	[	0.000	–	0.071	]	0.018	[	0.000	–	0.052	]	0.010	[	0.000	–	0.031	]	0.027	[	0.000	–	0.089	]	0.025	[	0.000	–	0.088	]	–					
	floating M6.2	0.000	[	0.000	–	0.000	]	0.000	[	0.000	–	0.000	]	0.000	[	0.000	–	0.000	]	0.000	[	0.000	–	0.000	]	0.000	[	0.000	–	0.000	]	–					
	float. M6.2 on CS+CC	0.000	[	0.000	–	0.000	]	0.000	[	0.000	–	0.000	]	0.000	[	0.000	–	0.000	]	0.000	[	0.000	–	0.000	]	0.000	[	0.000	–	0.000	]	–					
Concord/GV	CON	0.001	[	0.000	–	0.014	]	0.001	[	0.000	–	0.013	]	0.001	[	0.000	–	0.007	]	0.002	[	0.000	–	0.019	]	0.002	[	0.000	–	0.017	]	–					
	GVS	0.000	[	0.000	–	0.005	]	0.000	[	0.000	–	0.004	]	0.000	[	0.000	–	0.002	]	0.001	[	0.000	–	0.007	]	0.001	[	0.000	–	0.007	]	–					
	CON+GVS	0.003	[	0.000	–	0.017	]	0.003	[	0.000	–	0.013	]	0.002	[	0.000	–	0.008	]	0.005	[	0.000	–	0.022	]	0.004	[	0.000	–	0.021	]	–					
	GVN	0.000	[	0.000	–	0.001	]	0.000	[	0.000	–	0.001	]	0.000	[	0.000	–	0.001	]	0.000	[	0.000	–	0.001	]	0.000	[	0.000	–	0.001	]	–					
	GVS+GVN	0.004	[	0.000	–	0.025	]	0.003	[	0.000	–	0.018	]	0.002	[	0.000	–	0.011	]	0.006	[	0.000	–	0.032	]	0.005	[	0.000	–	0.031	]	–					
	CON+GVS+GVN	0.027	[	0.000	–	0.103	]	0.024	[	0.000	–	0.076	]	0.014	[	0.000	–	0.046	]	0.038	[	0.000	–	0.135	]	0.036	[	0.000	–	0.127	]	–					
	floating M6.2	0.000	[	0.000	–	0.000	]	0.000	[	0.000	–	0.000	]	0.000	[	0.000	–	0.000	]	0.000	[	0.000	–	0.000	]	0.000	[	0.000	–	0.000	]	–					
San Greg.	SGS	0.021	[	0.000	–	0.103	]	0.019	[	0.000	–	0.059	]	0.011	[	0.000	–	0.037	]	0.028	[	0.000	–	0.127	]	0.027	[	0.000	–	0.124	]	–					
	SGN	0.039	[	0.000	–	0.175	]	0.034	[	0.000	–	0.097	]	0.020	[	0.000	–	0.060	]	0.065	[	0.000	–	0.281	]	0.049	[	0.000	–	0.212	]	–					
	SGS+SGN	0.026	[	0.000	–	0.101	]	0.025	[	0.000	–	0.060	]	0.015	[	0.000	–	0.039	]	0.041	[	0.000	–	0.144	]	0.032	[	0.000	–	0.117	]	–					
	floating M6.9	0.020	[	0.008	–	0.037	]	0.023	[	0.010	–	0.039	]	0.013	[	0.006	–	0.023	]	0.023	[	0.010	–	0.039	]	0.023	[	0.010	–	0.039	]	–					

Greenville	GS	0.007 [0.000 – 0.029]	0.007 [0.000 – 0.019]	0.004 [0.000 – 0.012]	0.009 [0.000 – 0.039]	0.008 [0.000 – 0.037]	–						
	GN	0.010 [0.000 – 0.034]	0.010 [0.000 – 0.023]	0.006 [0.000 – 0.014]	0.013 [0.000 – 0.046]	0.011 [0.000 – 0.042]	–						
	GS+GN	0.014 [0.001 – 0.039]	0.014 [0.006 – 0.025]	0.008 [0.003 – 0.015]	0.019 [0.000 – 0.057]	0.017 [0.000 – 0.051]	–						
	floating M6.2	0.000 [0.000 – 0.000]	0.000 [0.000 – 0.000]	0.000 [0.000 – 0.000]	0.000 [0.000 – 0.000]	0.000 [0.000 – 0.000]	–						
Mt Diablo	MTD	0.025 [0.000 – 0.083]	0.026 [0.000 – 0.070]	0.015 [0.000 – 0.040]	0.038 [0.000 – 0.129]	0.038 [0.000 – 0.127]	–						

It comes as no surprise that the choice of probability model for calculating the regional earthquake probability has a significant effect on the result (**Figures 6.7, 6.8**). Relative to the Poisson model, with mean regional probability of a **M**≥6.7 earthquake of 0.60 [0.51 – 0.70], the corresponding BPT-step model mean probability is elevated (0.69 [0.54 – 0.87]), while that of the Empirical model is suppressed (0.45 [0.32 – 0.58]), in accord with the observed low post-1906 regional seismicity rate. While the difference between mean regional probability for the Poisson and BPT models is small compared to their respective spreads, the empirical calculations stand distinctly apart, with mean probability outside the 95% confidence range of both these probability models. The distribution of regional probabilities calculated with the weighted probability models reflect these differences, with the Empirical and BPT models defining, respectively, the lower and upper bounds of an approximately flat distribution (**Figure 6.7b**). Thus, the formidable spread in the weighted results (~0.4 to ~0.9) largely reflects our uncertainty about how the 1906 stress change affected the SFBR faults. If we could set aside this part of the problem (i.e., consider just one probability model, as was done in WG88 and WG90), uncertainty in the regional probability would be approximately halved.

The importance of the choice of probability model (including the choice of treatment of the interaction effects) can also be seen in results for the individual faults (**Figure 6.8)**. On the San Andreas fault, the mean probability calculated for the Time-Predictable model is the highest. The Empirical and BPT model probabilities are both suppressed, relative to the Poisson, but for different reasons: the Empirical model result reflects the observed low seismicity rates, while the BPT model results reflect the recency of the segment-resetting 1906 earthquake on the San Andreas fault.

Choice of fault rupture model

We characterized each major fault system in the SFBR with a set of fault rupture models. Each rupture model describes a possible mode of long-term behavior of a fault in terms of the size, location and relative frequencies of the ruptures occurring on it. Each fault was described by a set of up to 5 alternate rupture models (**Chapter 3**), with the assignment of weights to alternate rupture models reflecting a diversity of views within the expert panels concerning the strength of the fault segment barriers and long-term rupture behavior. Here we explore the sensitivity of the 30-year probabilities to the assignment of weights to these models. For a benchmark, we use the 30-year probability of a **M**≥6.7 earthquake calculated for a Poisson probability model using the expert-determined weights for the rupture models. We compare the benchmark to a suite of corresponding calculations in which each rupture model is, in turn, assigned a weight of 1.0 (**Figure 6.9).**

For **M**≥6.7 earthquakes, the 30-year probability depends strongly on the choice of rupture model for the San Andreas and San Gregorio faults, but is relatively insensitive to the choice of rupture model for the Hayward-Rodgers Creek and Calaveras faults. On the San Andreas fault (**Chapter 3**), rupture model A (P=0.21) favors full 1906-type ruptures, which decreases the moment available for (and, hence, rate of) smaller (**M**~7) earthquakes. In contrast, fault rupture model D for the San Andreas (P=0.28) gives the least weight to 1906-type ruptures, and so increases the rate of the smaller-magnitude 1- and 2-segment ruptures. Model D was given the least weight

(0.08) by the experts. On the San Gregorio fault, model C is the greatest contributor of **M**≥6.7 earthquakes because the combined SGN-SGS rupture is not allowed in this model, so all the available moment is consumed in the production of single-segment and floating rupture sources.

Choice of M–log A relation

We estimated the mean magnitude of each rupture source from its seismogenic area. A great deal of earthquake physics is included in this step, much of it only poorly understood. Empirical models (e.g., Wells and Coppersmith, 1994) and empirically fit theoretical models (e.g., Hanks and Bakun, 2001) often are used for this purpose. We considered five alternate **M**–log *A* relations in determining the mean magnitude, **M,** for each rupture source, based on its area, A, and seismogenic scaling factor, R (**Table 4.1**). It is evident in **Figure 4.2** that the available relevant observations do not clearly rule out any of these models. The uncertainty in the choice of the **M**–log *A* relation is an example of epistemic uncertainty in the model, and is formally incorporated into the model through branch weights obtained via expert opinion.

For any given rupture source (except those corresponding to **M**>7.7 earthquakes) the mean magnitudes given by the various **M**–log *A* relations differ by at most 0.2 magnitude units (**Figure 4.2**). This difference corresponds to a factor of ~2 in seismic moment and has a significant impact on earthquake rates and probabilities of occurrence. **Figure 6.10** shows the dependence on the choice of **M**–log *A* relation of the 30-year probability (calculated with the weighted probability model) of a **M**≥6.7 earthquake on each fault and in the region. Illustrative of the sensitivity to this modeling step is the consistent relationship between probabilities calculated with Model 1b (**M**=log *A* + 4.2) and Model 1a (**M**=log *A* + 4.1). Model 1b produces larger magnitude earthquakes and (because the fault models are slip rate-balanced) lower occurrence rates and probability, while Model 1a produces smaller magnitude earthquakes and, thus, higher rates and probability. Overall, the uncertainty associated with the choice of **M**–log *A* relation contributes a significant, but not dominant, portion of the total uncertainty in probability.

Accounting for aseismic slip

We accounted for aseismic slip through the use of the *seismogenic scaling factor*, *R*, which varies from *R*=0 (all slip occurs aseismically) to *R*=1 (all slip occurs in earthquakes). Expert groups estimated a range of values of *R* for each segment of the region's faults (**Table 4.1**, **Appendix B**). We considered two ways of accounting for aseismic slip in the regional earthquake model: R could scale the area of the fault segment that slips in earthquakes, or R could scale the slip rate of the segments. A combination of these approaches is permitted in the calculation sequence. We concluded that *R* should be used solely to scale the area, and so assigned this approach a weight of 1.0 in its calculations (see discussion in appendix). **Figure 6.11** compares the long-term frequency-magnitude relations for the San Andreas, Hayward-Rodgers Creek, Calaveras and Concord-Green Valley faults calculated using area scaling and slip rate scaling. Accounting for aseismic slip with either method lowers the earthquake potential of the fault, relative to a model that ignores creep. On the Calaveras fault, for example, slip rate scaling and area scaling for aseismic slip reduce the rate of **M**≥6.7 earthquakes by factors of approximately 2.5 and 3, respectively (**Figure 6.11**). This effect is small for locked faults, larger for creeping faults.

In addition to the choice of scaling method used, uncertainty in the *value* of the seismogenic area factor, *R*, also contributes to uncertainty in the calculated earthquake probabilities. **Figure 6.12** shows the 30-year probability of **M**≥6.7 earthquakes on the Hayward-Rodgers Creek and Calaveras faults calculated using, in turn, the lower, weighted, and upper value for *R* in Table 4.1, and *R*=1.0. Not surprisingly, the probability of characterized ruptures increases with decreasing amounts of aseismic slip.

Estimate of the aperiodicity, α, in earthquake recurrence.

Inherent variability in the intervals between successive events (i.e., aperiodicity) introduces aleatory uncertainty in the probability calculation, which is represented in the BPT models by the parameter α. In addition, epistemic uncertainty in the model arises from the fact that the value of α is not precisely known.

In **Chapter 5**, we considered some of the issues involved in estimating α, and saw that pertinent paleoseismic and seismological data are sparse and require careful interpretation in order to make such estimates. Based on an analysis of available data (Ellsworth and others, 1999), we constrained α for the BPT model calculations to be in the range 0.3 to 0.7 and placed greater weight on the upper end of the range. The sensitivity of the 30-year probabilities to the value of α over this range is illustrated in **Figure 6.13**, but is perhaps more fundamentally understood in terms of the hazard function for the BPT models (**Figure 5.8b**). The effect of α on earthquake probability on a fault segment depends on the segment's phase in its earthquake cycle. At times early in the cycle, the hazard *increases* with increasing values of α. At these times, increasing the aperiodicity increases randomness, thus diminishing the importance of the fault's cyclic behavior and raising the probability toward its long-term level. For example, on the San Andreas fault, all of whose segments are near the beginning of their current cycle (which began in 1906), increasing α *increases* the 30-year conditional probability.

At times later in the cycle (after ~1 mean recurrence time), hazard *decreases* with increasing values of α. At these times, increasing the randomness in the process diminishes the importance of the "ripeness" or "overdue" nature of the fault associated with cyclic behavior at advanced times and lowers the probability toward its long-term level. For example, on the Hayward-Rodgers Creek and Calaveras faults, where the time since the last resetting events is comparable to or greater than the mean recurrence time for several of their segments, increasing α *decreases* the 30-year conditional probability. Overall, the regional sensitivity to α is dominated by those faults that are late in their cycles, especially the Hayward-Rodgers Creek and Calaveras faults.

Because our probability calculations integrate hazard over a 30-year period and combine the weighted contributions from five probability models, the dependence of probability on α seen in **Figure 6.13** is diluted, relative to its dependence in a pure BPT calculation.

Summary of sensitivity tests

As discussed in **Chapter 5**, the greatest source of uncertainty in our probability calculations is in the choice of probability model. The distribution of regional probabilities calculated with the

Poisson probability model includes all the sources of uncertainty arising in the fault characterization steps (**Figure 6.7a**). Added to this uncertainty is the uncertainty associated with the time-dependent probability models. The BPT and Empirical models each make additional assumptions and introduce additional uncertainty that broaden the distribution of the calculated regional probability (**Figure 6.7a**). However, the greatest source of uncertainty is in the choice *among* these probability models – a choice in which we found no clearly preferred candidate (**Figures 5.11, 6.7b**). Future efforts to estimate earthquake probability for the SFBR will benefit most from an improved understanding of the factors controlling the timing of earthquake occurrence and, in particular, the effects of fault interactions (see **Chapter 8**).

Within the long-term fault characterization model, the choice among the alternate fault rupture models is a major source of uncertainty for some faults. The assumptions involved in our model of fault segmentation – both in the definition of the fault segments and in the ways in which fault segment ruptures may combine in earthquakes – have a strong effect on the probabilities calculated on the San Andreas and San Gregorio faults.

Finally, on the Calaveras and Hayward faults, which sustain a significant amount of aseismic slip, the assumption of how aseismic slip affects the production of earthquakes is significant (**Figure 6.11**). Although we assume that aseismic slip on fault segments reduces their seismogenic area, an alternative interpretation (reduction in their long-term slip rate) can result in a significant change in the earthquake probabilities estimated for these faults.

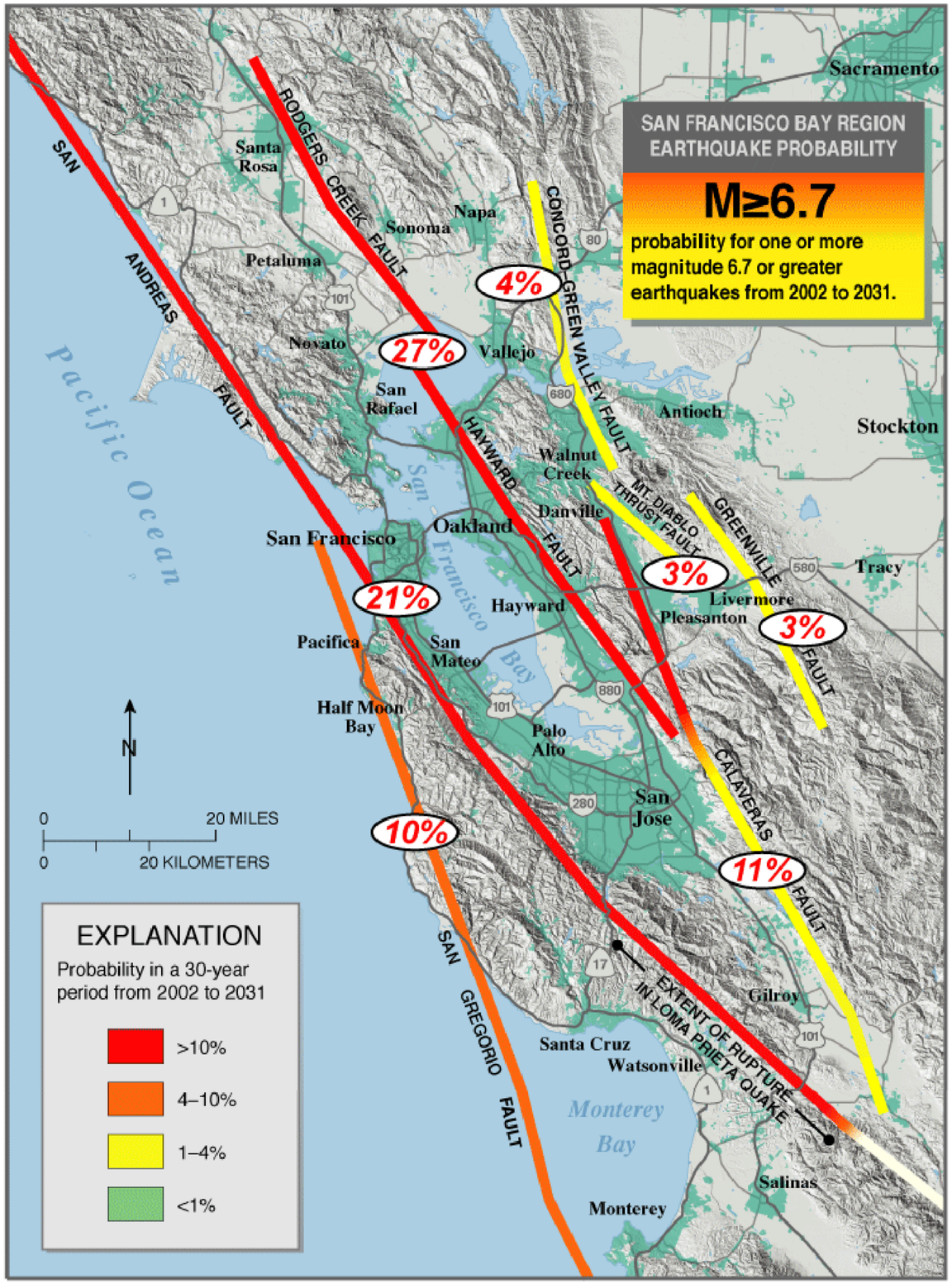

(a)

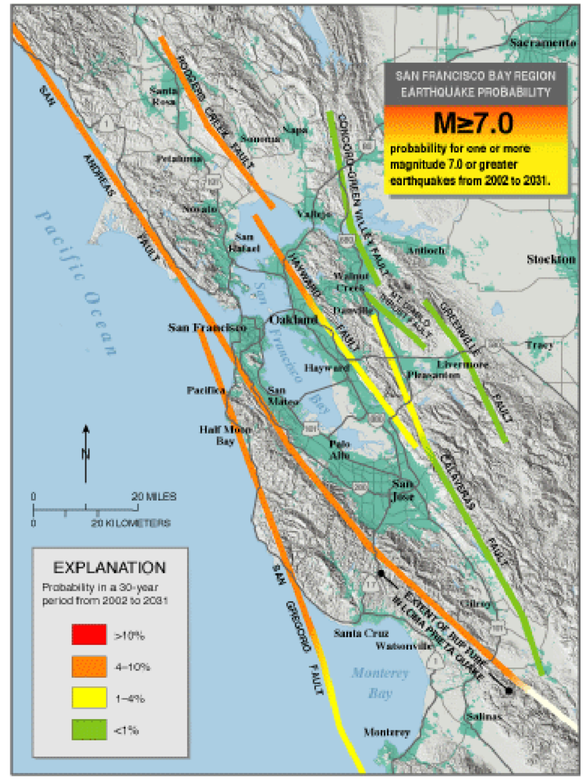

(b)

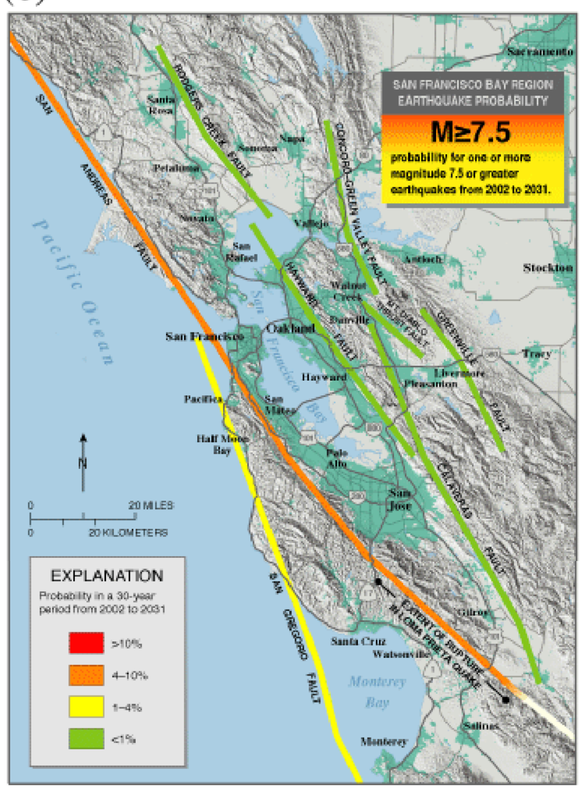

(c)

Figure 6.1. Probabilities of one or more strong earthquakes occurring on faults in the SFBR during the next 30 years. a) Earthquakes with M≥6.7. Probability of occurrence on each fault is indicated in ovals. Colors indicate the corresponding probabilities for each fault segment. b) Earthquakes with M≥7.0. c) Earthquakes with M≥7.5. The probability of earthquakes decreases with increasing earthquake magnitude (see Table 6.1).

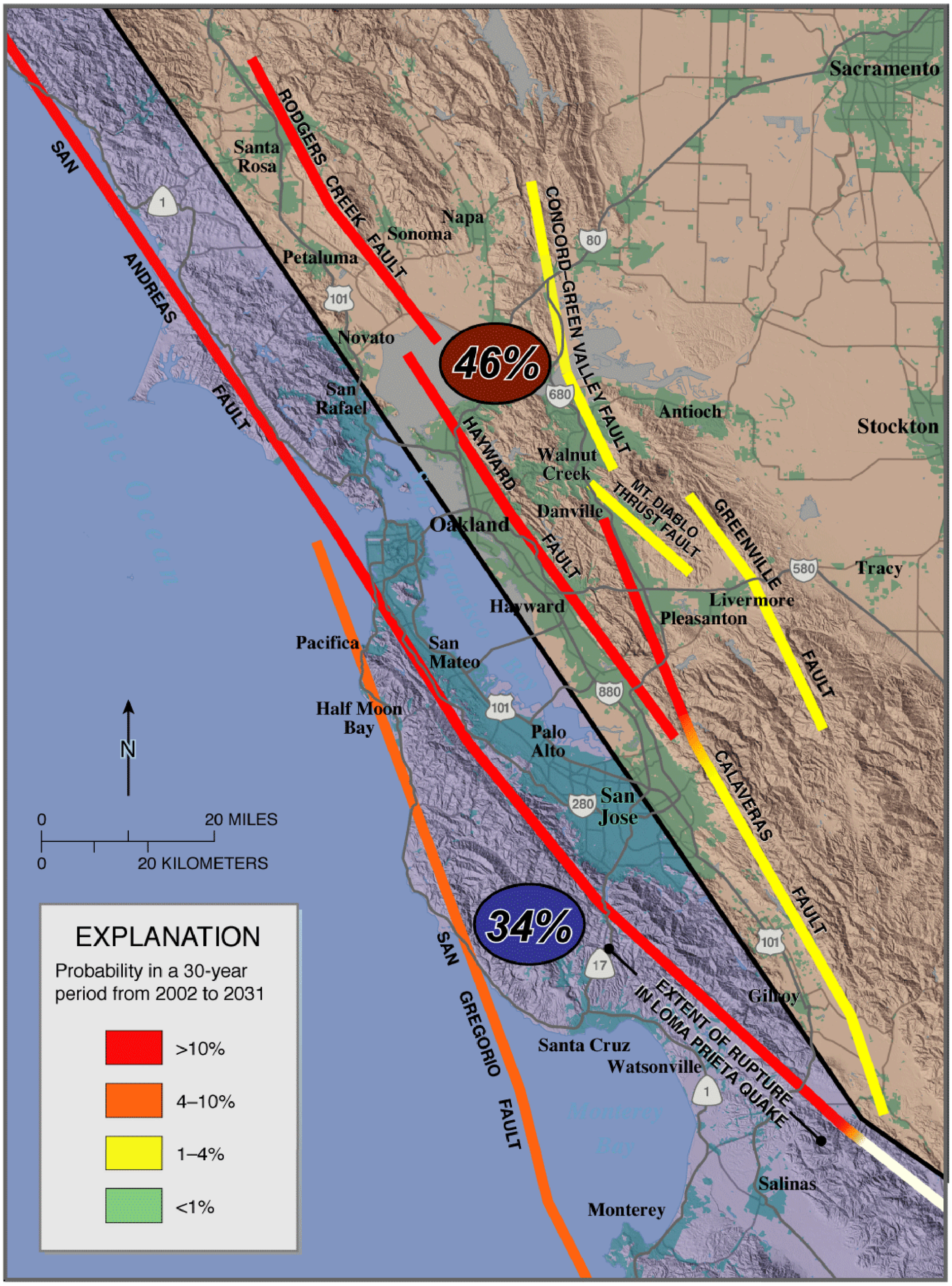

Figure 6.2. Geographic distribution of probability of M≥ 6.7 earthquakes in the next 30 years. Black line separates sub-regions northeast and southwest of San Francisco Bay. The combined probability in the northeast sub-region (including the faults within it and one-half the background probability) is 0.46. In the southwest sub-region, the corresponding combined earthquake probability is 0.34.

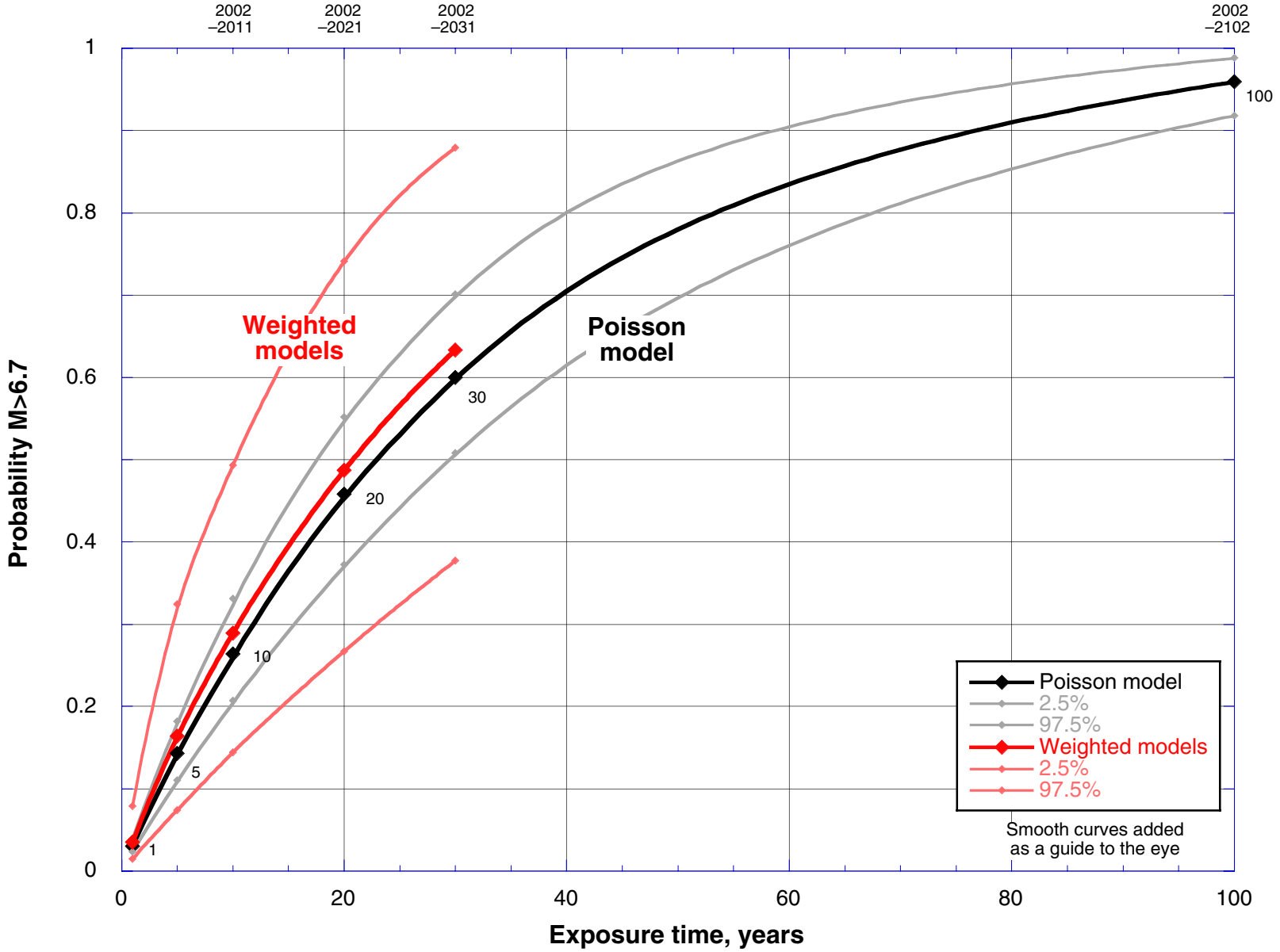

Figure 6.3. Probability of M≥6.7 earthquakes in the SFBR calculated for time intervals ("exposure times") of 1, 5, 10, 20, 30, and 100 years. All intervals begin in 2002. Calculations are shown for the weighted set of probability models (red) and for the Poisson model (black).

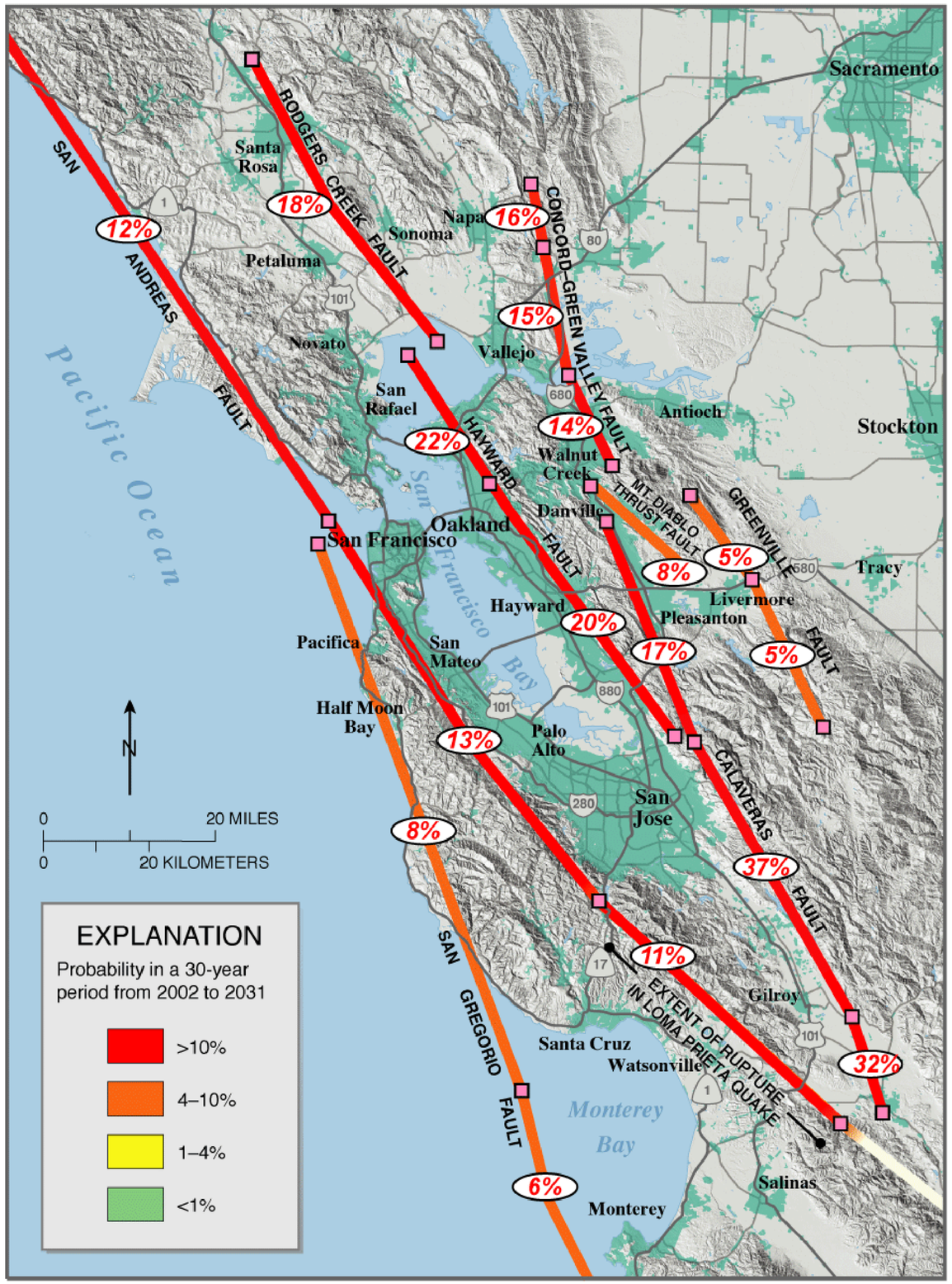

(a)

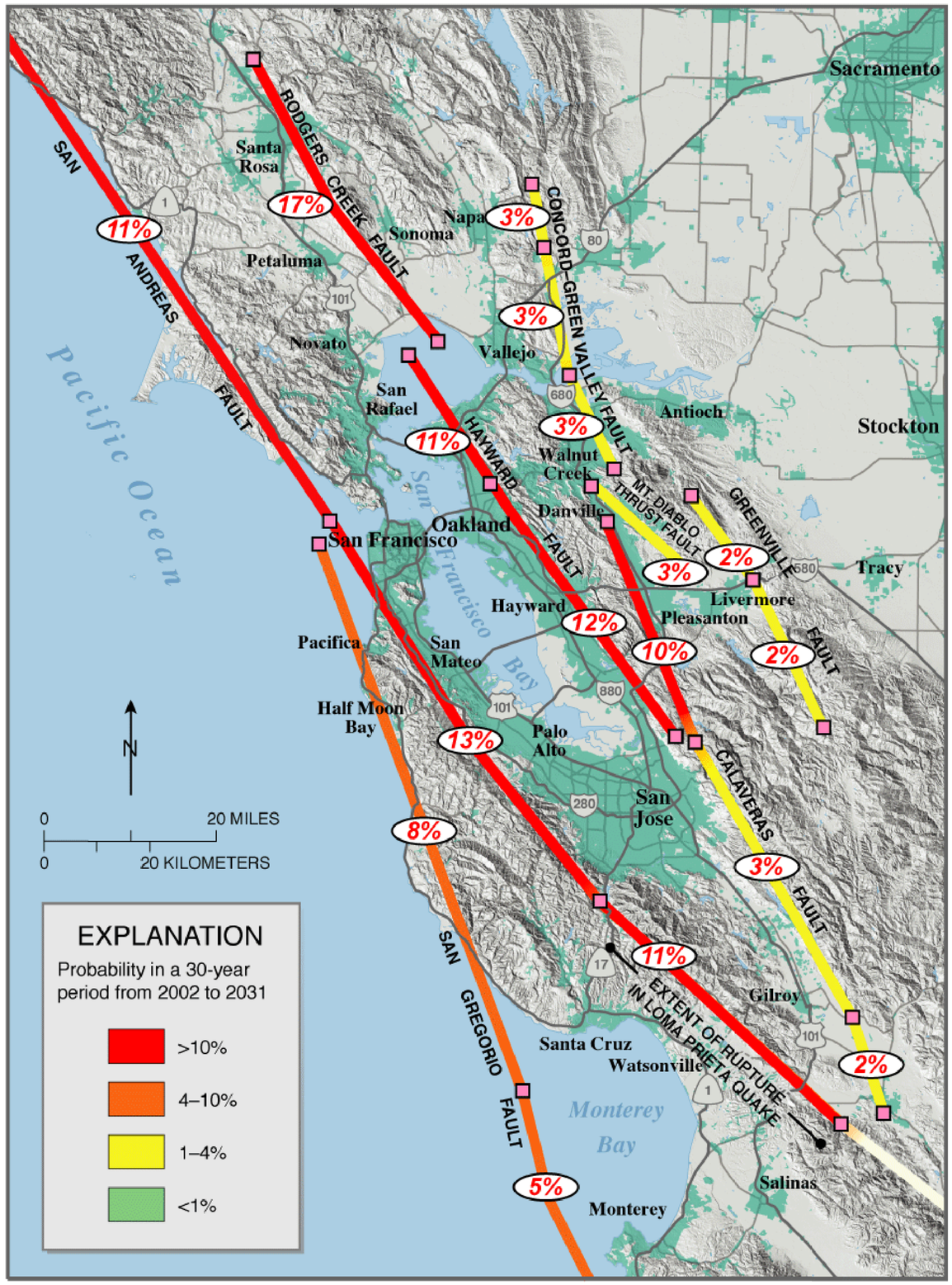

(b)

Figure 6.4. Probabilities of fault segment ruptures during the next 30 years. a) all characterized ruptures; b) M≥6.7 ruptures. Probabilites and uncertainties are listed in Table 6.3. Pink boxes are segment boundaries.

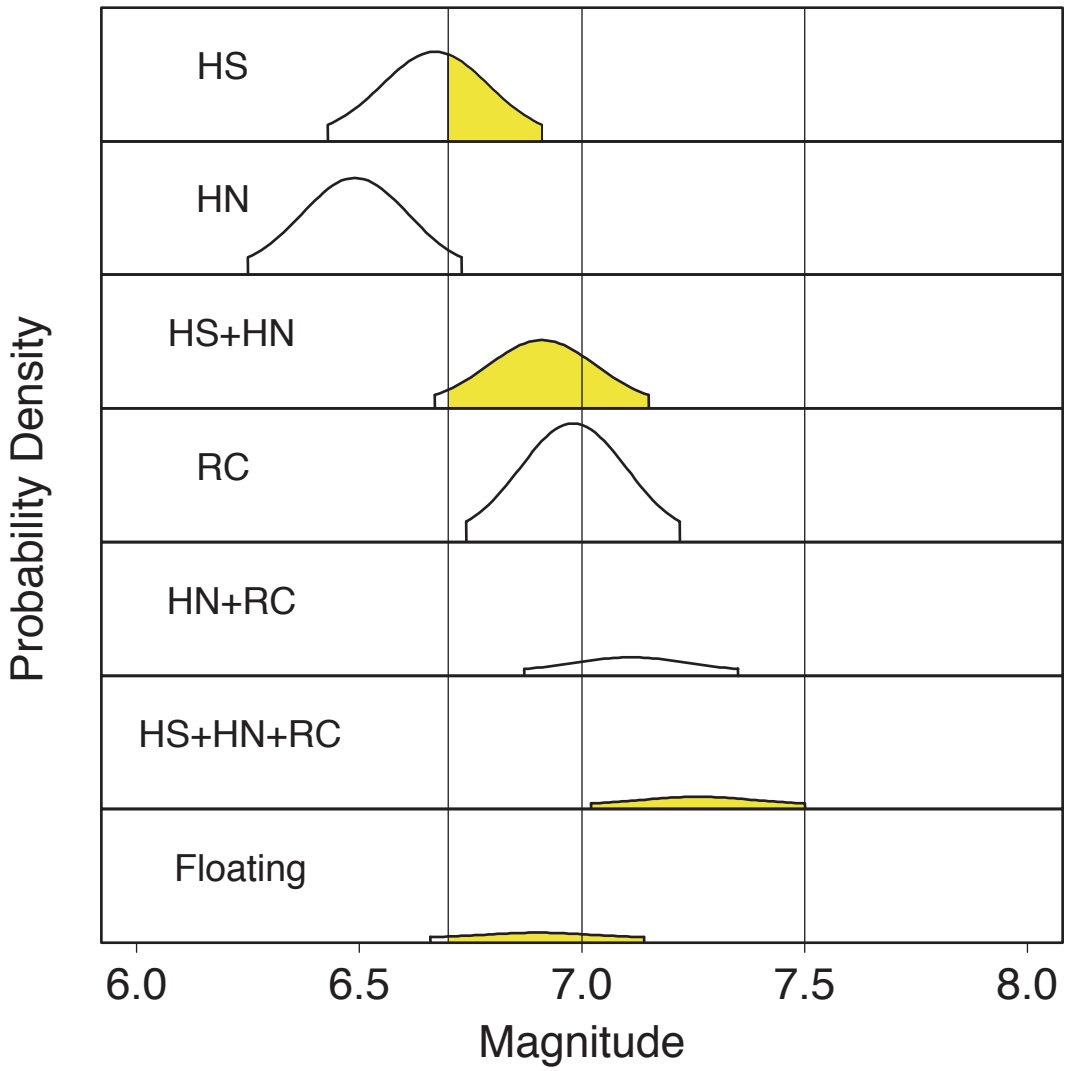

Figure 6.5. Probability density functions for rupture sources on the Hayward-Rodgers Creek Fault. The width of these truncated Gaussian distributions represents the alleatory uncertainty in magnitude of ±0.24 assumed for each rupture source. Mean magnitudes are listed in bottom portion of Table 6.5. The probability of rupture on a given fault segment (given in Table 6.3) is the combined area under the curves for the rupture sources involving that segment. Corresponding segment probability for ruptures above a magnitude threshold is combined areas to the right of the threshold magnitude. For example, color indicates the probability of a rupture of segment HS in M>6.7 earthquakes. (The contribution from the Floating source is a portion of the colored area proportional to the length of the segment.) Epistemic uncertainty is not included in this illustration. Vertical lines indicate M>6.7, M>7.0 and M>7.5 magnitude thresholds.

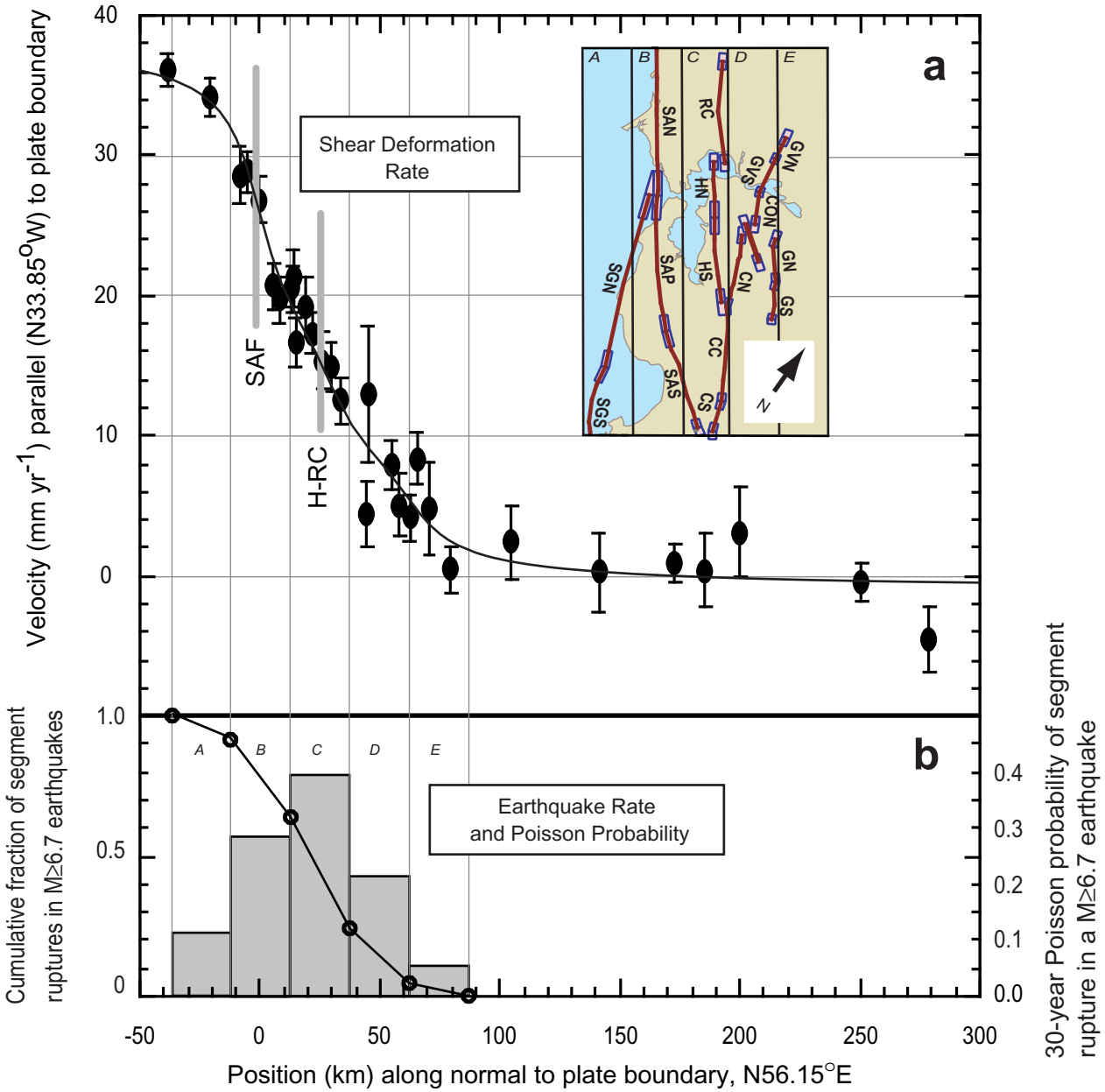

Figure 6.6. Comparison of contemporary rate of shear deformation and calculated earthquake rate and probability across the SFBR. (a) Motion of geodetic stations parallel to the Pacific-North American plate boundary (N33.85° W), taken from Prescott et al. (2001) is shown by solid dots with 2-sigma error bars. Smooth curve is the deformation predicted by the best fitting model of Prescott et al. (2001). (b). Solid points and connecting lines show the cumulative fraction (scale on left) of the regional rate of segment ruptures in the WG02 long-term model occurring in 25-km-wide swaths (labeled *A* through *E* in inset) parallel to the San Andreas fault. One-fifth of the background rate was assigned to each swath, even though some background events (and the Mt. Diablo thrust) do not contribute to shear deformation. Gray bars show the 30-year Poisson probability (scale on right) of a segment rupture in a M≥6.7 earthquake occurring in the same 25-km-wide swaths.

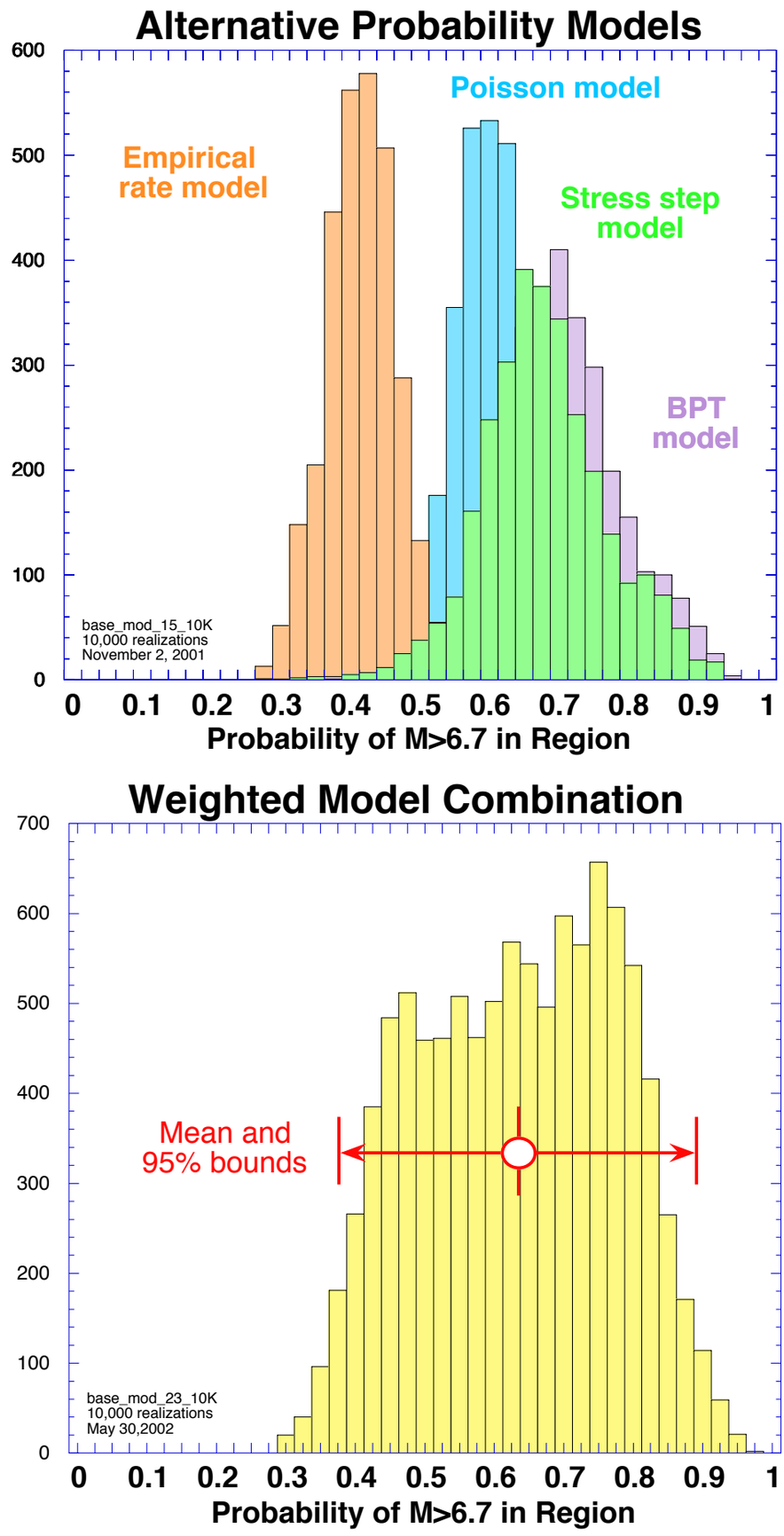

Figure 6.7. Distributions of the regional probability of a M 6.7 earthquake calculated using various probability models. a) Overlapping histograms show probability calculated in 3000 iterations using each of four models separately. The shape and width of each distribution reflects epistemic uncertainty in the choice of underlying models and parameters. b) Corresponding distribution calculated in 10,000 iterations using the weighted combination of models described in the text and shown in Figure 5.12. The broad shape of this distribution reflects the combination of distinct behaviors of he alternate models. Additional mass near P=0.8 corresponds to realizations that employ the Time-Predictable model on the San Andreas fault, not shown in (a).

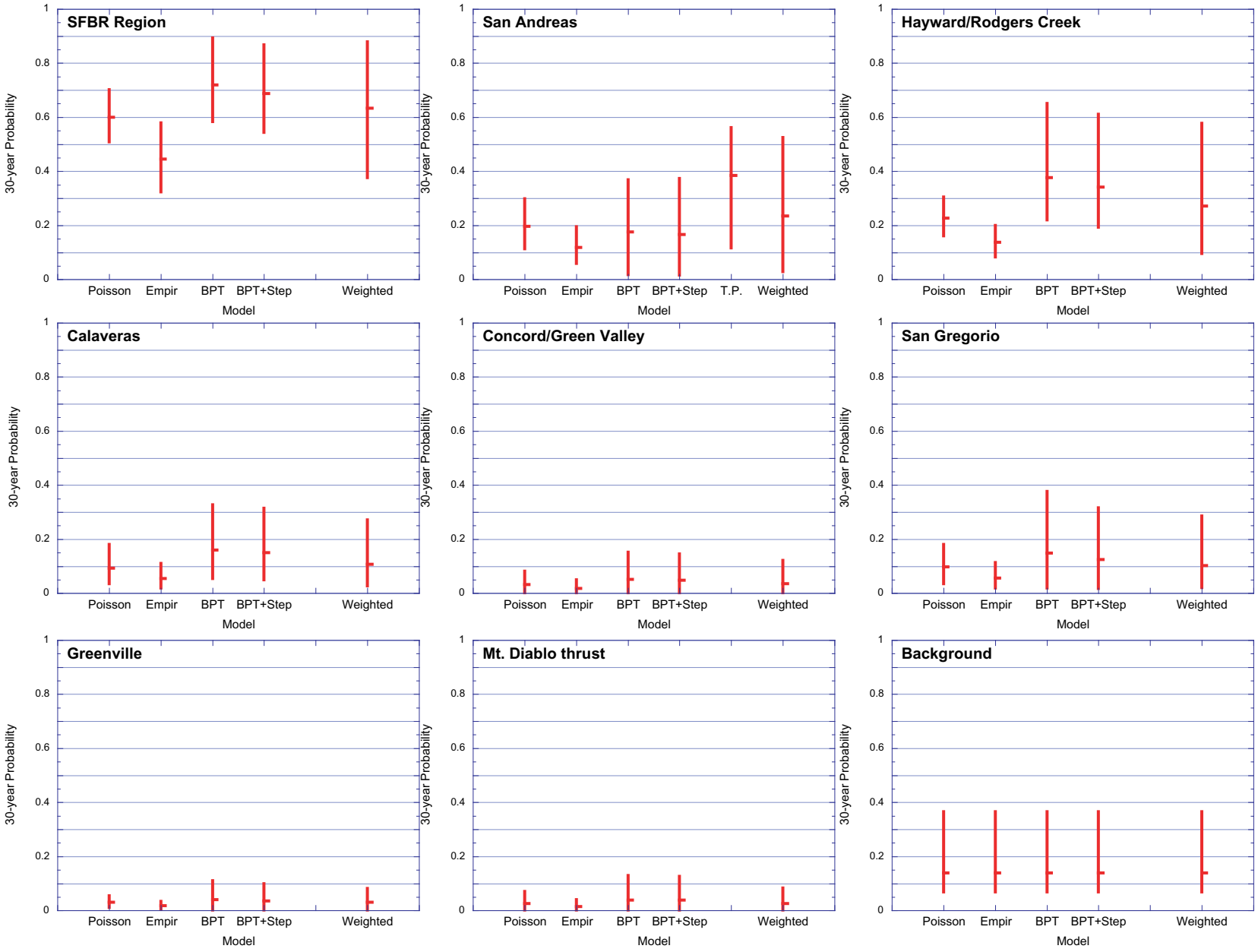

Figure 6.8. Conditional probabilities of one or more M≥6.7 earthquakes in the region, on each characterized fault, and in the background. Probabilities calculated for each probability model and for the weighted combination of models are shown (see Table 6.15). Mean probability is indicated by horizontal tick, and 95% confidence range by full length of bar.

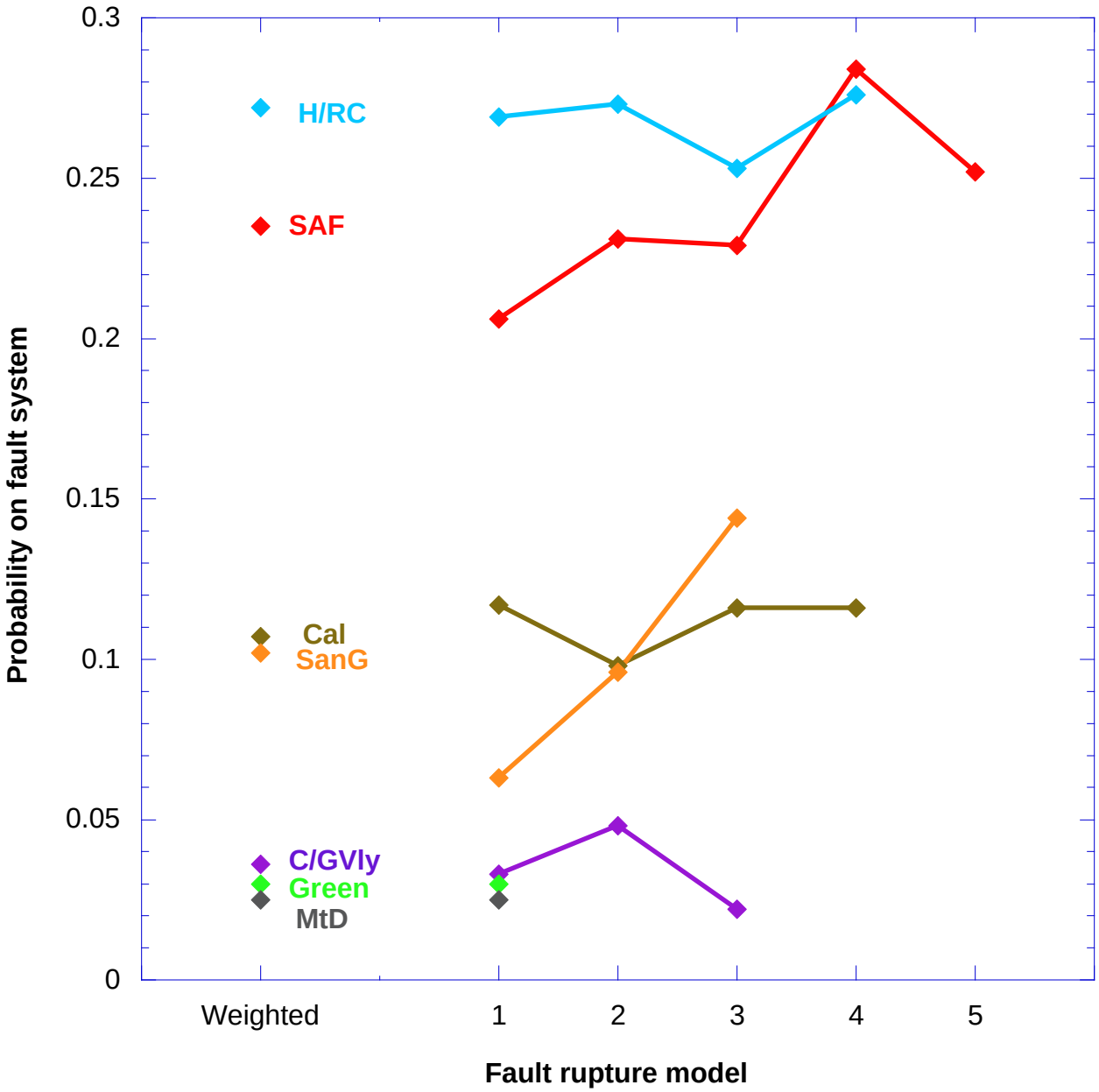

Figure 6.9. Dependence of earthquake probability on the choice of fault rupture model. See Chapter 2(?) for definitions of the fault rupture models. All calculations are for M≥6.7 earthquakes (2002-2031) on a single fault system and use the weighted probability model. Benchmark calculations (points on left) use rupture model weights adopted by WG02. Connected points are corresponding probabilities for the cases in which 100% weight is given, in turn, to each of the individual rupture models. H/RC=Hayward-Rodgers Creek fault; Cal=Calaveras fault; SanG=San Gregorio fault; SAF=San Andreas fault; C/Gvly=Concord-Green Valley fault; Green=Greenville fault; MtD=Mount Diablo fault.

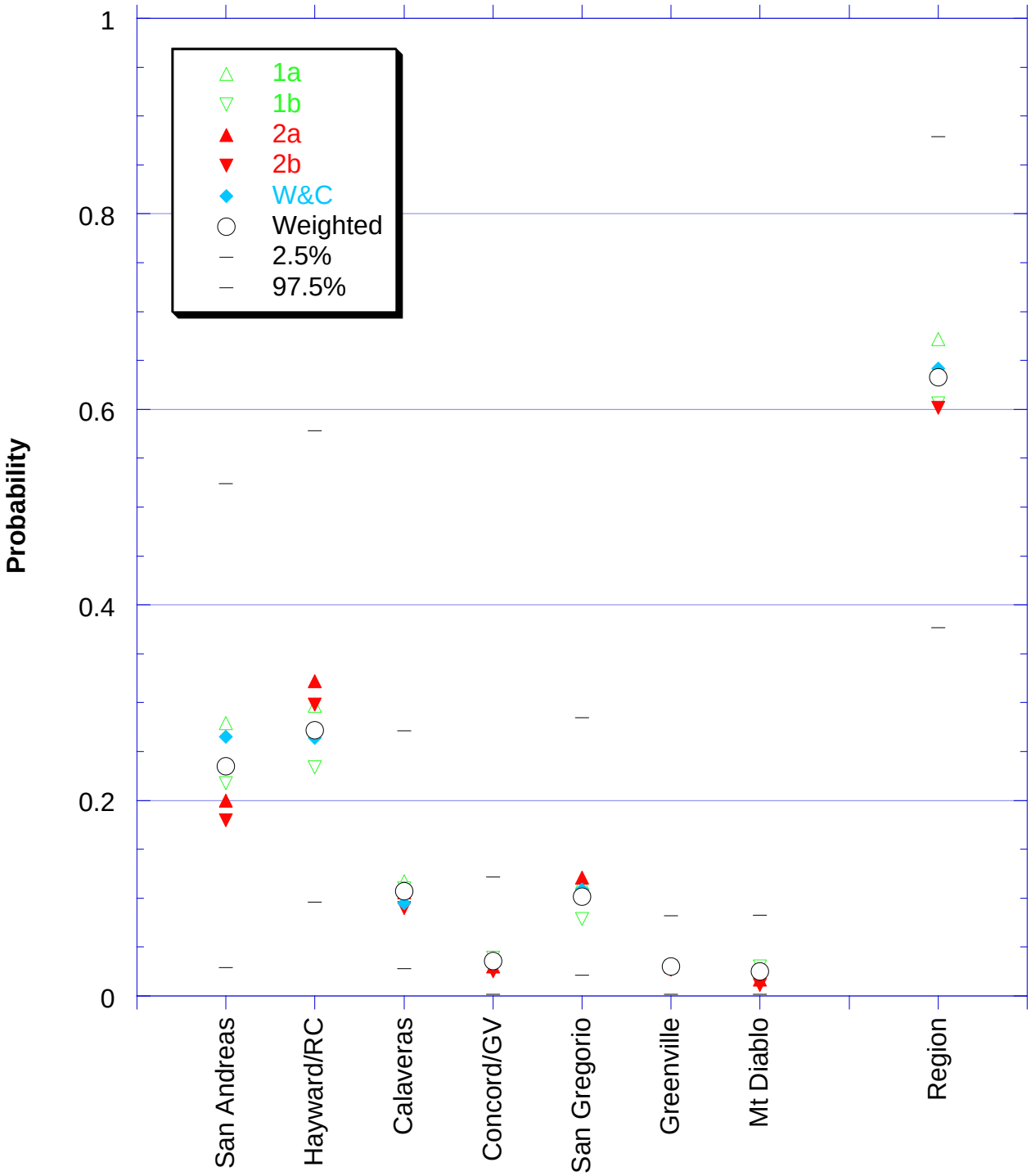

Figure 6.10. Dependence of probability on the choice of **M**-log A relation. See Equations 4.4 to 4.6 for definitions of the **M**-log A relations. All calculations are for M≥6.7 earthquakes in 2002-2031. Benchmark calculations (black circles) and their 95% confidence range (black bars) were calculated using the weights for the **M**-log A relations given in Table 4.2. Colored symbols represent the corresponding probabilities calculated with100% weight assigned, in turn, to each **M**-log A relation.

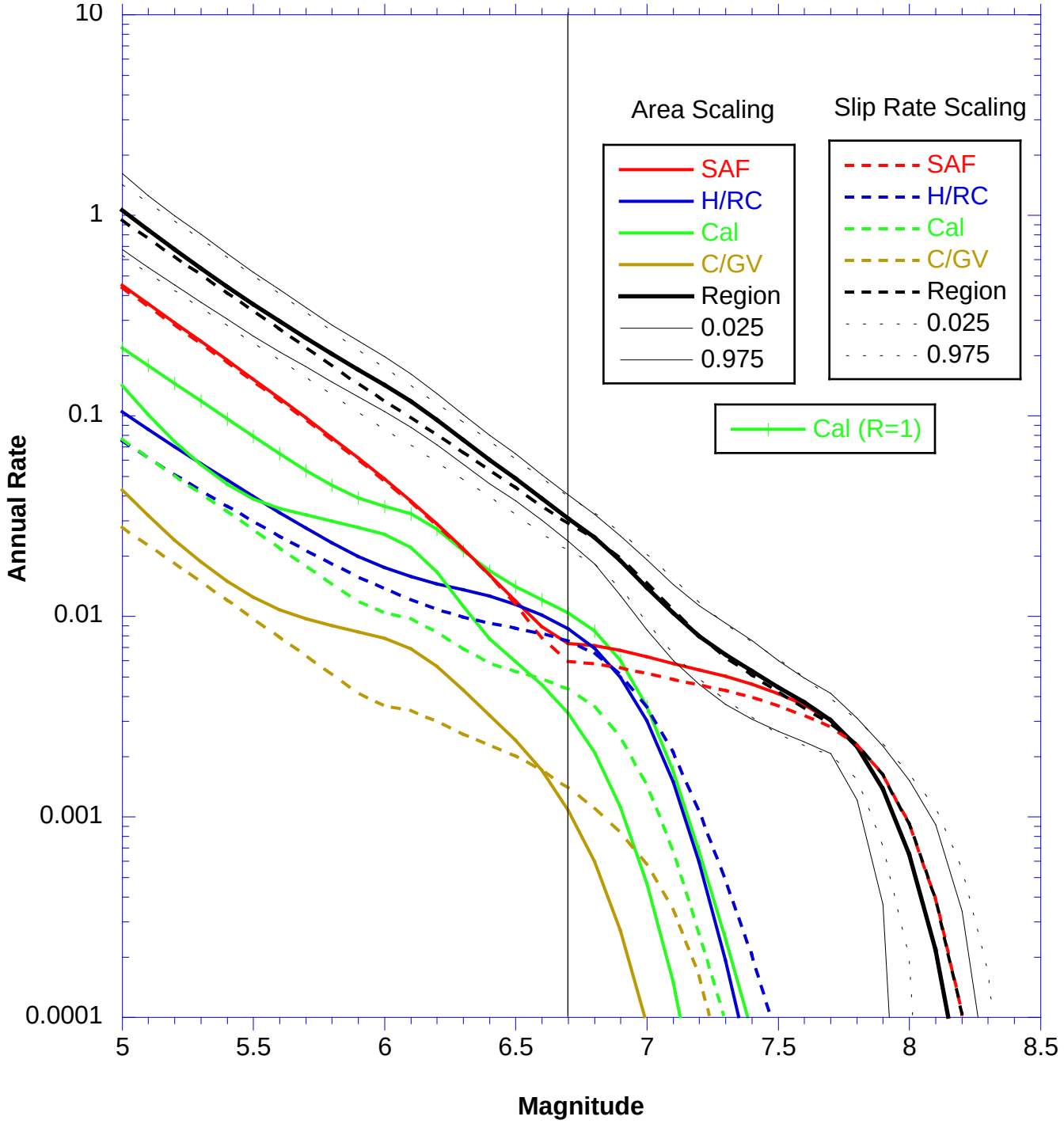

Figure 6.11. Dependence of the modeled earthquake rates on the method used in accounting for the aseismic slip (creep) on four selected faults and in the region. The frequency-magnitude relations for each fault and the region are shown for the case in which aseismic creep reduces the rupture area of each rupture source (solid lines) and the case in which aseismic creep reduces the long-term slip rate available for earthquakes (dashed lines). Hatchured green line shows frequency-magnitude distribution for the Calaveras fault without any accounting for aseismic slip (i.e., R=1.0). Calculations are for M>6.7 earthquakes in 2002-2031.

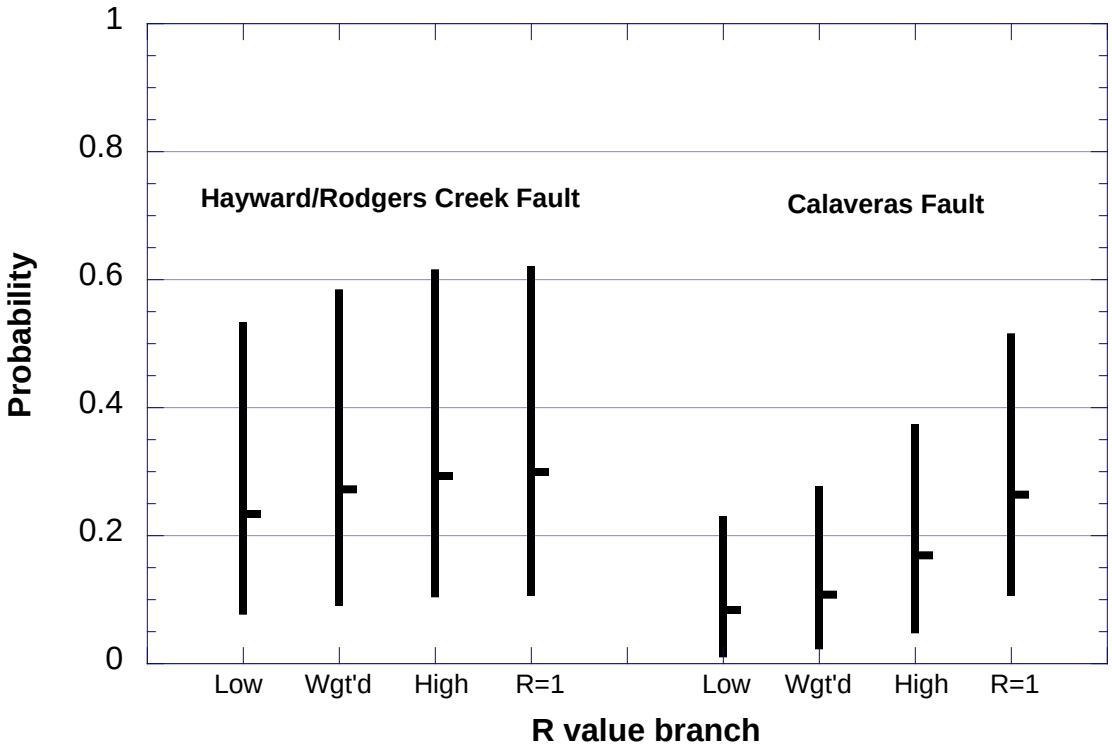

Figure 6.12. Dependence of probability on the seismogenic scaling factor, R. Calculations are for **M≥**6.7 earthquakes (2002-2031) on the Hayward-Rodgers Creek and Calaveras faults. "Low ", "Wgt'd", High" and "R=1" correspond to the lower, weighted, and upper values of R given in Table 4.1 and to R=1.0. Horizontal bars are mean values, vertical bars show the 95% confidence range.

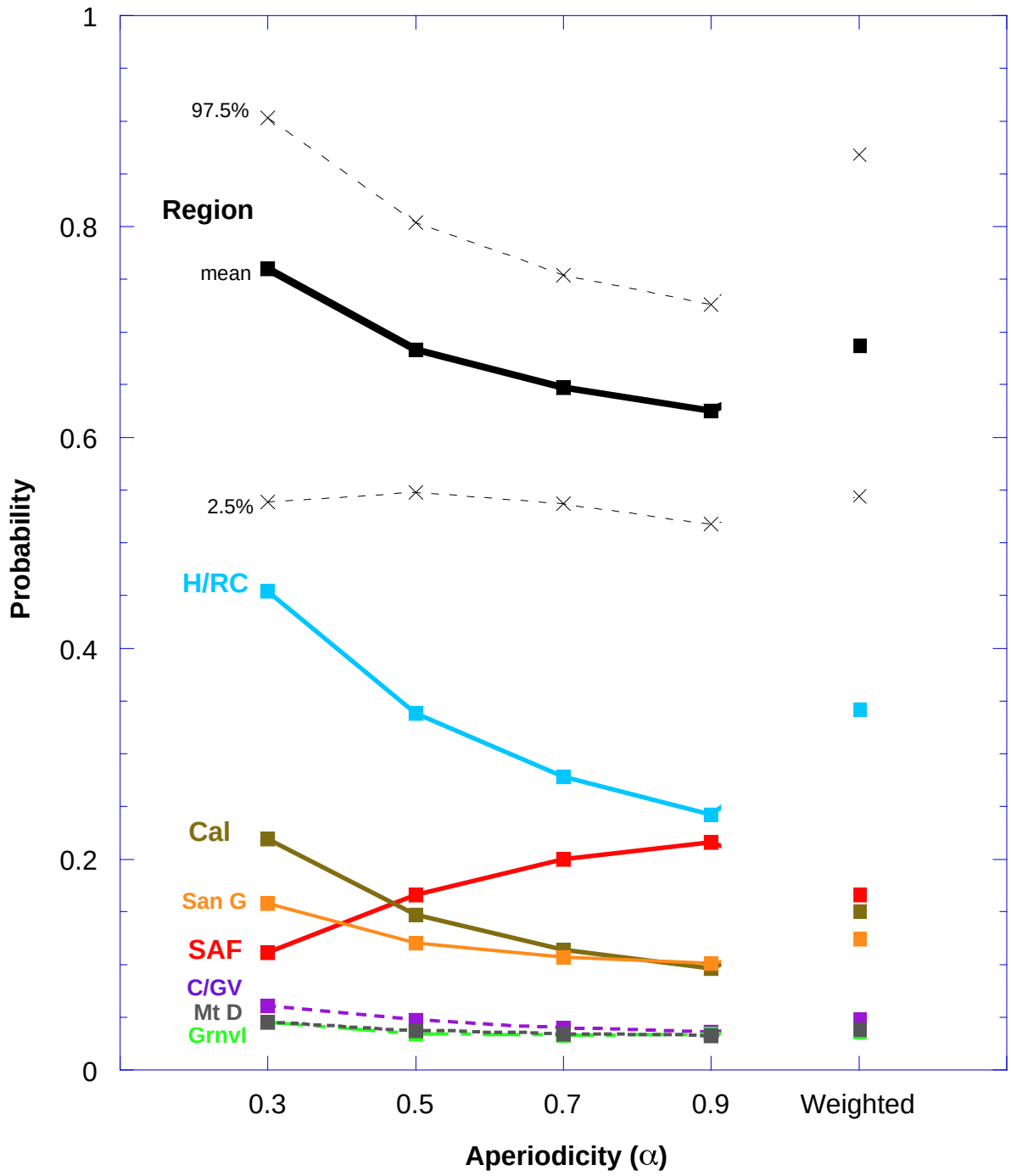

Figure 6.13. Dependence of earthquake probability on the value of the aperiodicity parameter, a, used in the BPT-step model. All calculations are for M>6.7 earthquakes (2002-2031) on individual fault systems and in the region. Points on right are probabilities for faults and the region calculated with the weights for α adopted by WG02. Connected points are the corresponding probabilities calculated with 100% weight given, in turn, to each of four values of α. Black dashed lines and crosses show 95% confidence range for the regional probability calculations.